

**Tephrochronology of core PRAD 1-2 from the Adriatic Sea: insights into  
Italian explosive volcanism for the period 200-80 ka**

A.J. Bourne<sup>1\*</sup>, P.G. Albert<sup>2\*</sup>, I. P. Matthews<sup>1</sup>, F. Trincardi<sup>3</sup>, S. Wulf<sup>4</sup>, A. Asioli<sup>5</sup>, S.P.E  
Blockley<sup>1</sup>, J. Keller<sup>6</sup> J.J. Lowe.<sup>1</sup>

<sup>1</sup> Centre for Quaternary research, Department of Geography, Royal Holloway University of  
London, Egham, Surrey, TW20 0EX, U.K.

<sup>2</sup> Department of Earth Sciences, Royal Holloway University of London, Egham, Surrey,  
TW20 0EX, U.K.

<sup>3</sup> ISMAR-CNR, Istituto di Scienze Marine-Consiglio Nazionale delle Ricerche, Via Gobetti,  
101 40129, Bologna, Italy

<sup>4</sup> GFZ German Research Centre for Geosciences, Section 5.2 – Climate Dynamics and  
Landscape Evolution, Potsdam Germany

<sup>5</sup>Istituto di Geoscienze e Georisorse del C.N.R.- Sede di Padova, c/o Dipartimento di  
Geoscienze dell'Università di Padova, C.so Garibaldi, 37 35121 Padova, Italy

<sup>6</sup>Institute of Geosciences, Mineralogy – Geochemistry, Albert-Ludwigs-University Freiburg,  
Albertstrasse 23b 79104 Freiburg, Germany

\*Present address: Department of Geography, College of Science, Swansea University,  
Singleton Park, Swansea, SA2 8PP.

Email address [a.j.bourne@swansea.ac.uk](mailto:a.j.bourne@swansea.ac.uk)

## **Abstract**

Core PRAD 1-2, located on the western flank of the Mid-Adriatic Deep, was investigated for tephra content within the part of the sequence assigned on biostratigraphic and sapropel-layer stratigraphy to MIS 5 and 6 (ca. 80 - 200 ka BP). A total of 11 discrete tephra layers are identified, 8 visible and 3 cryptotephra layers. 235 geochemical measurements obtained from individual glass shards using WDS-EPMA enabled 8 of the 11 tephras to be correlated to known eruption events, 4 of which are represented in the Lago Grande di Monticchio (LGdM) regional tephra archive sequence. Three of these layers are recognised distally for the first time, extending their known distributions approximately 210 km further north. The results provide an independent basis for establishing an age-depth profile for the MIS 5 - 6 interval in the PRAD 1-2 marine record. This approach allowed age estimates to be interpolated for the other five tephra layers that could not be correlated to known events. It also provides an independent test of, and support for, the broad synchronicity of sapropel-equivalent (S-E) events in the Adriatic Sea with the better-developed sapropel layers of the eastern Mediterranean, proposed by Piva et al. (2008a).

## **1. Introduction**

Recent studies of Central Mediterranean tephra layers dating to between 130 and 90 ka (e.g. Calanchi and Dinelli, 2008; Caron et al., 2010; Giaccio et al., 2012; Paterne et al., 2008; Regattieri et al., 2015; Vogel et al., 2010; and Wulf et al., 2012) have revealed the large number of layers potentially available for the synchronisation of marine sequences over this time period (Figure 1). This previous body of work also generated a robust geochemical dataset obtained from glass shards, building on results previously reported by Keller et al. (1978) and Paterne et al., (1986, 1988) for sites in the Ionian and Tyrrhenian Seas (Figure 1).

These studies provide base-line information for classifying the tephra layers and assigning them to source eruptions. However, the number of tephra layers for this period that have been identified in terrestrial sequences is much greater than has so far been reported from marine records: for example, 21 tephra events have been identified in the Lago Grande di Monticchio sequence that date to between 100 and 130 ka BP (Wulf et al., 2012) whereas only 6 tephra layers have been detected in Central Mediterranean marine cores for the same interval (Paterne et al., 2008). Whilst this may reflect more limited dispersal or different transport pathways of some of the eruptions, it might also result from the sampling strategy employed in the analysis of marine cores, if focused only on the detection of visible traces of tephra or on the analysis of glass shards found when sieving for foraminifera tests. An investigation of marine sediments from core site PRAD1-2 in the Central Adriatic utilising cryptotephra extraction techniques (based on Blockley et al., 2005), however, found that of a total of 25 discrete tephra layers dating to within the last 105,000 years, only one was visible, the other 24 being cryptotephra layers, not visible to the naked eye or detectable by routine down-core scanning (Bourne et al., 2010).

Here we report the results of an investigation of a part of the PRAD 1-2 sediment sequence that lies below that previously reported, and which spans the MIS-5 and MIS-6 intervals. The aims of the investigation were to (1) undertake a comprehensive examination of this part of the sequence to establish the number of discrete cryptotephra and visible tephra layers represented; (2) chemically characterise each layer using major element and trace element analytical methods where applicable; (3) compare the results with available geochemical information reported for eruptive deposits from both the proximal setting and from key marine (e.g. Ionian, Tyrrhenian and Adriatic Seas) and terrestrial (e.g., Lago Grande di Monticchio) distal ash archives from the central Mediterranean; (4) identify key tephra layers

with robust age estimates; (5) develop an age-depth profile for this part of the PRAD 1-2 core sequence and (6) use this age-depth profile to independently test the chronology of palaeoceanographic events proposed by Piva et al., (2008 a,b).

For the time period of interest, the construction of marine chronologies has tended to rely heavily on alignment of stratigraphic changes with dated terrestrial records (e.g. Sánchez Goñi et al., 2002) or on orbital calibration (e.g. Lourens, 2004); both approaches restrict the potential to detect and assess the magnitude of phase differences between the records, whereas using tephra layers as isochrones to link the records can reveal significant phase differences between them (Davies et al., 2012). The key criteria that enable tephra layers to serve as useful and reliable isochrones are: (1) they are robustly geochemically characterised and are geochemically distinctive from other tephra layers; (2) they can be traced widely and are registered in a number of different archives; (3) they are securely dated; (4) they help to constrain the age or age equivalence of key events or features, such as sapropel layers. The degree to which the tephra layers reported in this study meet these criteria is assessed below.

## **2. Site Context**

Core PRAD 1-2 was recovered from the western and upper flank of the Mid-Adriatic Deep at Lat. 42°40'34.7826"N, Long. 14°46'13.5565"E, where water depth is 185.5 m (Figure 2). This location was selected for coring because a major seismic survey of this part of the Adriatic revealed a series of sub-parallel seismic reflectors and uniform seismic units in this vicinity (Ridente et al., 2008). The recovered core sequence comprises 71.2 m of continuous sample (99.96% core recovery). Piva et al. (2008a and b) undertook a multi-proxy study of the core sequence which allowed the recognition of marine isotope stages, sapropel-equivalent events



and magnetic excursions, providing a stratigraphic framework and preliminary age control for the core sequence. Sapropel-equivalent events are characterised by low  $\delta^{18}\text{O}$  and  $\delta^{13}\text{C}$  values, minima in magnetic parameters, low colour reflectance and a foraminiferal assemblage that is characteristic of that seen in Eastern Mediterranean sapropel units (Figure 3). The record in the upper part of the sequence extending to MIS-5.1 and including sapropel-equivalent layer 1 (S-E1) was reported in Bourne et al. (2010). Key stratigraphic information for the part of the core sequence investigated here, which spans MIS-5 and MIS-6 and includes S-E3 to S-E6, is summarised in Figure 3. Further details are provided in Piva et al. (2008a and b). Interpretations of the sedimentological, isotope and foraminiferal data of Piva et al., (2008 a and b) are not re-examined in this study. Instead, our principal aim is to generate an age model for the sequence that is independent of assumed alignments, in order to test the chronology of events they have previously been proposed.

### **3. Tephrostratigraphical Methods**

#### ***3.1 Tephra extraction***

Contiguous 5 cm-long sub-samples were extracted from throughout the entire core sequence shown in Figure 3 and sieved to recover all sediment particles between 125 and 25 microns in size. The sieve mesh was changed regularly to avoid cross-contamination. This fraction was then immersed in sodium polytungstate of prepared density following the procedures set out in Blockley et al. (2005), using a cleaning float of  $1.95 \text{ gcm}^{-3}$  and an extraction float of  $2.50 \text{ gcm}^{-3}$ . The supernatant of the extraction float was mounted on glass slides in Euparal and scanned for presence of glass shards under an optical microscope fitted with cross-polarising filters. The numbers of shards were then counted and concentrations per gram of sample (dry weight) calculated.

### ***3.2 Labelling of tephra layers***

Individual discrete tephra layers are assigned a unique code. For non-visible tephra layers, the code refers to the depth in the profile at which peak glass shard concentration was detected in the sequence; for example, PRAD 2605 denotes peak shard concentration at 2605 cm depth. For visible layers, the unique code denotes the position of its visible base (2525 cm for PRAD-2525). This approach is preferred to an ordinal classification, as it reduces confusion and potential ambiguity should additional tephra layers be detected in subsequent research (Lowe, 2011).

### ***3.3 Geochemical analysis of glass shards***

Between 2375 and 3065 cm all tephra layers identified (both visible and cryptotephra layers) were selected for geochemical analysis. Beyond 3065 cm only visible tephra layers and cryptotephra layers with greater than 500 glass shards were geochemically analysed as there was a more constant and higher background of tephra shards than in the younger sections of the core. For those tephra layers selected for geochemical analysis, glass shards extracted from the layers were mounted in Struers Epofix epoxy resin. Mounts were sectioned and polished and checked using reflected light microscopy. Chemical analysis of vitreous material was undertaken using wavelength-dispersive spectrometry electron probe microanalysis (WDS-EPMA) to ensure compatibility with other key data-sets (see below). Analysis of the majority of the samples was carried out using a Cameca SX100 microprobe (housed at the Department of Geosciences, University of Edinburgh) operated with a defocused 5 µm beam size, 15 kV voltage and 2 nA current for Na K, Si, Al, Mg, Fe and Ca or 80 nA current for F, Cl, S, Mn, Ti and P (Hayward, 2012). Two samples, PRAD-2605 and PRAD-2812, were analysed using a JEOL JXA-8800R microprobe (housed at the

Department of Earth Science, Oxford University), with a defocused 10  $\mu\text{m}$  beam size and 10nA current. The beam count time for individual elemental analyses was 40s but this was reduced to 10s for Na to avoid element mobilisation. Both machines were calibrated using modified standard blocks supplied by the instrument manufacturers while a combination of internally-assayed Lipari and StHs6/80-G (Jochum et al., 2005, 2006) were used as secondary standards.

The data were screened for non-glass material and outlier values and samples with analytical totals less than 95% were excluded (Hunt and Hill, 1993). Analyses were normalized on all biplots to an anhydrous state (i.e. 100% total oxides) for data comparison. The raw geochemical results, including data obtained from standards, are provided in the supplementary data.

For some tephra layers grain-specific trace element analyses were undertaken using laser-ablation inductively-coupled plasma mass spectrometry (LA-ICP-MS). Analyses of distal tephra deposits were performed using an Agilent 7500es ICP-MS coupled to a Resonetics 193nm ArF excimer laser-ablation analyser (housed in the Department of Earth Sciences, Royal Holloway, University of London) following the analytical procedures of Tomlinson et al. (2010). Spot sizes of 25 and 20 $\mu\text{m}$  were used depending on the vesicularity and/or size of glass shard surfaces. The repetition rate was 5 Hz and the count time 40 s on the sample and 40 s on the gas blank to allow the subtraction of the background signal. Blocks of eight samples/shards of glass and of one MPI-DING reference glass standard were bracketed by measurements obtained using the NIST612 glass calibration standard (GeoREM 11/2006).

The internal standard used was  $^{29}\text{Si}$  (determined by EPMA analysis). Geochemically distinct MPI-DING (Jochum et al., 2006) reference glass standards were used to monitor analytical accuracy, these covering the potential geochemical spectrum observed within tephra deposits. For consistency we used the same secondary standards as were used for EPMA analysis. LA-ICP-MS data reduction was performed in accordance with Tomlinson et al. (2010), using Microsoft Excel. Accuracies of analyses of ATHO-G and StHs6/80-G MPI-DING glass are typically  $\leq 5\%$ . Relative standard errors (% RSE) for tephra samples using a 25  $\mu\text{m}$  spot size are typically  $<3\%$  for V, Rb, Sr, Y, Zr, Nb, Ba, La, Ce, Pr, Nd, U;  $<6\%$  for Sm, Eu, Dy, Er, Th; and  $<20\%$  for Gd, Yb, Lu, Ta. Percentage RSE increases with smaller spot sizes (see Supplementary data). Full errors (standard deviations and standard errors for individual sample analyses) are given in the supplementary information.

### ***3.4 Tephra Correlation***

The EPMA results obtained from this study were first compared with the comprehensive geochemical data-sets available from the Lago Grande di Monticchio archive (Wulf et al., 2012) and with data-sets published for tephra records obtained from sites in the Sulmona basin and along the Cilento coastline (Giaccio et al., 2012; Regattieri et al., 2015). Additional comparisons were also subsequently attempted with data obtained from Adriatic core RF95-7 (Calanchi and Dinelli, 2008), from Ionian Sea cores (Keller et al., 1978; Insinga et al., 2014) and from Lake Ohrid (Vogel et al., 2010; Caron et al., 2010; Sulpizio et al., 2010). Some of these data-sets were obtained using EDS SEM systems that differ significantly from the WDS-EPMA system employed in the present study, although Sulpizio et al. (2010) showed that EDS and WDS measurements conducted on the same samples differed by less than 1% for elements with greater than 0.5 wt% abundance. We therefore confine our comparisons with the EDS SEM data to the most abundant elements only.

#### 4. Results

**PRAD-2375** has a peak of 217 shards  $\text{g}^{-1}\text{dw}$  (per g dry weight), with a vertical distribution of glass shards over 5 cm. The shards are clear and intermediate but some show evidence of alteration, such as hydration rims on intermediate shards (Figure 4a). This layer was originally described by Bourne et al. (2010) but could not be assigned to a known volcanic eruption because only a few scattered geochemical data points were available. Additional geochemical data for this layer has been obtained here and indicates that there are 2 main populations that comprise this layer. The first is a Na-pronounced trachyte with  $\text{SiO}_2$  concentrations ranging from 65.88 – 70.52 % and  $\text{NaO}_2$  concentrations ranging from 5.12 – 6.90 % (Figure 5). The other population is of trachyphonolite composition, with a high alkali ratio (HAR) (average  $\text{K}_2\text{O}/\text{Na}_2\text{O} = 1.75$ ) (Figure 5) and  $\text{SiO}_2$  concentrations ranging from 58.20 – 68.63 %.

**PRAD-2525** is visible in the core, with a base at 2525.5 cm depth. The visible layer has a thickness of 10 cm, but when associated cryptotephra components are taken into account, the layer has an overall thickness of 46 cm, with a maximum peak glass shard concentration at 2517 cm. The shards are predominantly clear and fluted (Figure 4b). Geochemical data obtained throughout the entire vertical distribution of glass shards proved homogenous throughout. The layer is trachyphonolitic in composition (Figure 5) with  $\text{SiO}_2$  concentrations ranging from 58.72 - 61.21 % and a HAR, average  $\text{K}_2\text{O}/\text{Na}_2\text{O} = 1.85$ . This tephra was originally reported in Bourne et al. (2010) as PRAD-2517, the depth corresponding to the peak in glass shards and not the base of the visible layer. Additional trace element analyses and other new glass data from the top and bottom of this tephra layer are presented in the

Supplementary Data. The trace element data show minor variability (e.g.  $326 \pm 22$  ppm Zr ( $2\sigma$ );  $30 \pm 3$  ppm Th ( $2\sigma$ ), LREE enrichment relative to the HREE ( $\text{La/Yb} = 27.8 \pm 2.3$ ;  $2\sigma$ ).

**PRAD-2605** is a cryptotephra layer comprising glass shards with a vertical distribution of 15 cm and a peak concentration  $>10,000 \text{ g}^{-1} \text{ dw}$ . The layer is comprised only of clear shards which are predominantly fluted (Figure 4c). The geochemical data show the layer has a phonolitic chemistry (Figure 5), with  $\text{SiO}_2$  concentrations ranging from 59.01 – 60.04 % and an HAR affinity (average  $\text{K}_2\text{O}/\text{Na}_2\text{O} = 1.87$ ). Trace element concentrations in these glasses show limited compositional variability (i.e.,  $335 \pm 16$  ppm Zr ( $2\sigma$ );  $32 \pm 1$  ppm Th ( $2\sigma$ )), but LREE element enrichment compared to HREE ( $\text{La/Yb} = 28.2 \pm 1.9$ ;  $2\sigma$ ).

**PRAD-2812** comprises a visible layer 5 cm thick, but also a cryptotephra component that extends the overall vertical distribution to 25 cm. The maximum peak in glass occurs at 2805 cm, a little above the base of the visible layer. The geochemical data suggests this layer is trachytic (Figure 5), with  $\text{SiO}_2$  concentrations ranging from 61.61 - 62.55 %. (Figure 5) and showing a low alkali ratio (LAR) (average  $\text{K}_2\text{O}/\text{Na}_2\text{O} = 1.24$ ). Both the major and trace element glass data show bi-modality in glass composition (Figures 6, 7d, 8c and d). Consequently, incompatible trace element concentrations are heterogeneous within this tephra deposit (e.g. 407-1162 ppm Zr; 33-94 ppm Th) suggesting a mix of two distinct glass populations (Figure 8 c-d).

**PRAD-3065** is a cryptotephra layer with a peak of 843 shards  $\text{g}^{-1} \text{ dw}$ , of which 803 are clear and 40 are brown in colour. The shards have a vertical distribution of 5 cm and are predominantly platy, although some shards with closed vesicles are present (Figure 4e). It was not possible to obtain geochemical data for this layer, because three attempts to re-

sample the layer failed to recover glass shards. This might be due to discontinuous representation of the tephra layer, for micro-sedimentological studies of visible tephra layers in marine cores has shown that tephra can be horizontally discontinuous (Griggs et al., 2014), while multiple core studies of lake sediments have shown that sediment focussing can also make tephra layers laterally discontinuous (Davies *et al.*, 2007; Pyne-O'Donnell, 2011).

**PRAD-3225** comprises a visible layer which is 3.6 cm thick with a base at 3225.6 cm, while a cryptotephra component extends the vertical distribution of glass shards to 30 cm. Maximum shard concentration occurs at 3225 cm. Both platy and fluted shards are common which are nearly all clear, although a few brown shards were also observed (Figure 4f). Glass compositions range from phono-tephritic to a dominant phonolitic component, with SiO<sub>2</sub> concentrations ranging from to 51.91 - 60.38 % (Figure 5).

**PRAD-3336** is a 15 cm-thick cryptotephra layer with a peak of >10,000 shards g<sup>-1</sup>dw. The shards are predominantly platy (with large open vesicles), and clear (Figure 4g). The glass composition is phonolitic, with SiO<sub>2</sub> concentrations ranging from to 57.25 – 59.83 % (Figure 5).

**PRAD-3383** comprises a visible tephra layer which is 5.5 cm thick and has a base at 3383.5 cm, while a cryptotephra component extends the vertical distribution of glass shards to 30 cm, of which 5 cm lie below the start of the visible layer. The shard distribution is unimodal and the shards are highly fluted and vesicular, but also notable for possessing large closed vesicles (Figure 4h). Geochemical analysis classifies this layer as phono-trachytic with SiO<sub>2</sub> concentrations ranging from to 58.24 – 59.76 % (Figure 5).

**PRAD-3472** comprises a 3.1 cm-thick visible layer and a cryptotephra component that extends the vertical distribution of glass shards to over 15 cm. The shard distribution is unimodal and the dominant shard morphology is platy (Figure 4i). The shards are predominantly clear but the small number of brown shards present characteristically have a high concentration of small closed vesicles. Geochemical analysis classifies the layer as trachytic, with SiO<sub>2</sub> concentrations ranging from 61.34 – 64.77 % (Figure 5).

**PRAD-3586** comprises a 6.7 cm thick visible layer, while a cryptotephra component extends from the base of the visible layer to c. 30 cm above. The dominant shard morphology is platy and there are very few brown shards present (Figure 4j). Geochemical analysis on the 5-cm thick sample indicates a phonolitic composition, with SiO<sub>2</sub> concentrations ranging from 56.54 – 60.58 % (Figure 5).

**PRAD-3666** comprises a 14 cm-thick visible layer but with a cryptotephra component extending over 47 cm. There are also more brown shards present in this layer than in the others of a similar age and the shards are highly vesicular (Figure 4k). The layer is phonolitic with SiO<sub>2</sub> concentrations ranging from 57.86 – 58.94 % (Figure 5).

## **5. Tephra origins and correlations**

**PRAD-2375** is likely to originate from Pantelleria based on the alkali ratios (Figure 6a), the majority of which plot in this field. However, some shards show a closer affinity with the Campi Flegrei volcanic province. This mixed geochemical signal is likely to represent contemporaneous volcanic activity occurring at both Pantelleria and Campi Flegrei. Within the LGdM record, there is only one layer with a Pantelleria source, TM-22 (89.1 ± 4.5 ka)



which has been correlated to the Ignimbrite Z unit of Pantelleria (Wulf et al., 2004, 2012), formed by an eruption at c.  $85 \pm 1.7$  ka (Rotolo et al., 2013) (Figure 7a). PRAD-2375 glasses are compared to the compositions of Pantelleria off-shore marine layers spanning the last 200 ka (Tamburrino et al., 2012), and similarities support Pantelleria as the source of PRAD-2375 (Figure 7a), although no temporal correlation can be made with the layers recorded in the Sicily channel. TM-22 has also been related to the marine P-10 layer of Paterne et al. (1990) (Wulf et al., 2012). Within LGdM the layers of Campanian origin that lie closest to TM-22 are TM-22-1a and TM-22-1b which, although they have not been correlated more widely show close similarities to the Campanian population of PRAD-2375 (Figure 7a).

PRAD-2375 falls within a period of increased  $\delta^{18}\text{O}$  associated with MIS 5.2 stadial conditions (Figure 3) which is consistent with the occurrence of the P-10 tephra layer in core KET 80-04 (Paterne et al., 1988). The Pantelleria-type population within this layer appears to be geochemically distinctive during this time period, whilst also being stratigraphically well constrained. It therefore, has the potential to provide a crucial tephra marker if it is found in more archives.

**PRAD-2525** has an origin in the Campanian Volcanic Zone (CVZ) (Figure 6a). It also overlaps the average composition of the X-5 marine tephra layer (Figure 6b). Bourne et al. (2010) correlated this layer to TM-24 in the LGdM sequence, which was in turn correlated to the X-5 tephra by Wulf et al. (2004). The recent reappraisal of the LGdM record has seen the X-5 tephra reassigned to TM-25 (105.5 ka BP), a correlation which provides better geochemical and chronological agreement with the X-5 tephra (Giaccio et al., 2012; Wulf et al., 2012). Giaccio et al. (2012) correlate the Sulmona basin tephra level POP3 ( $106.2 \pm 1.3$  ka BP) to the LGdM TM-25 tephra and a stratigraphically younger Sulmona tephra level

POP1 ( $92.4 \pm 4.6$  ka) to the LGdM tephra TM-23-11. They also suggested that PRAD-2525 should be correlated to the younger LGdM tephra TM-23-11, rather than TM-24 as proposed by Bourne et al. (2010).

Given this important reappraisal of late MIS 5 tephras in the region and the recent release of new datasets (Giaccio et al., 2012; Wulf et al., 2012), PRAD-2525 can be reassessed in the light of the new trace element data. Major element data from PRAD-2525 overlap with the compositional fields of all the following LGdM tephras: TM-23-11/POP1, TM-24a/POP2, TM-24b/POP2a and TM-25/POP3/X-5 (Figure 7b-c). They differ, however, from the data published for the OT0701-7 and OT0702-8 layers from Lake Ohrid, which have been correlated to the X-5 tephra (Sulpizio et al., 2010). At the same time, the trace element glass data confirm that PRAD-2525 does not resemble the TM-25/POP3/X-5 tephra (Figure 8a). PRAD-2525 glasses lie on a separate evolutionary trend, best illustrated by Sr or Ce plotted against Th concentrations (Figure 8a). The PRAD-2525 glasses conform with the same evolutionary trend as LGdM tephras TM-24a and TM-24b, with respect to the same elements (Figure 8a). However, PRAD-2525 glasses can be easily distinguished from TM-24a and TM-24b glasses by more enriched incompatible trace element concentrations (i.e., Zr, Nb, Th) and lower LREE/Th ratios (Figure 8b).

The limited trace element data available for TM-23-11 do accord with the PRAD-2525 data (Figure 8a and b), which supports the correlation suggested by Giaccio et al. (2012). While trace element data for POP1 are not yet available to further test the POP1/TM-23-11 correlation, given that the stratigraphic position and major element glass data support the correlation of all three layers (PRAD-2525/TM-23-11/POP1), the POP1 age has been adopted in the age model.

350

351 **PRAD-2605** has the same compositional range as PRAD-2525 (Figure 7b-c), but is a discrete  
352 cryptotephra layer, separated by 80 cm of glass-free sediment. On the basis of major and  
353 trace element glass data PRAD-2605 is indistinguishable from the overlying visible tephra  
354 PRAD-2525 (Figure 7 b-c, Figure 8). Consequently, for the same reasons as those given  
355 above, a match between this cryptotephra and either the TM-25/X-5/POP3 or the younger  
356 TM-24 tephras must be rejected. This is supported by the stratigraphic position of PRAD-  
357 2605 as it occurs after Sapropel 4 whereas the X-5 occurs before sapropel 4 in marine cores  
358 and in environmental records with palaeoenvironmental changes linked to sapropels (Negri et  
359 al., 1999; Regattieri et al., 2015). Glass data suggests that a number of eruptions in the CVZ  
360 dispersed tephra with very similar major element geochemistries during this time period.  
361 Within the LGdM record, 19 tephra layers (representing 11 tephra events) greater than 0.5 cm  
362 in thickness lie between TM-22 and TM-24 all with overlapping major element geochemical  
363 signatures (Figure 9). Trace element analysis of these layers might, in due course, identify a  
364 correlative for PRAD-2605, but, until then, great care must be made when correlating tephra  
365 layers in this time period, for while some of the layers can be distinguished using trace  
366 element data (e.g. X-5/TM-25 and TM-24), others cannot (e.g. PRAD-2525/TM-23-11 and  
367 PRAD-2605). The issue of successive eruptions with similar glass compositions emitted by  
368 individual volcanic centres is not a new problem for tephrochronology (Lane et al., 2012;  
369 Caron et al., 2012); indeed, during the period 20 to 5 ka, the main CVZ eruptive centres of  
370 Campi Flegrei, Vesuvius and Ischia have generated numerous tephra layers with  
371 indistinguishable glass chemistries (Santacroce et al., 2008; Smith et al., 2011; Tomlinson et  
372 al., 2012; 2014). Hence additional information, such as careful assessment of stratigraphic  
373 position, is required to resolve matters further. However, additional problems include the  
374 poorly resolved chronology for some of the layers, while some may not be represented in the

proximal volcanic record. These considerations call into question whether some tephra layers emitted from the CVZ during this time frame are useful for correlation purposes.

**PRAD-2812** appears to also have an origin in the CVZ. Its bimodal, low alkali ratio (LAR) glass chemistry distinguishes it from the more frequently erupted HAR MIS-5 tephra layers derived from the CVZ. Interestingly some of the data obtained from PRAD-2812 cluster in the Ischia compositional field (Figure 6), in particular those of the field for the pre-Monte Epomeo Green Tuff (MEGT) (Figure 6). Based on major, minor and trace element data, PRAD-2812 can be correlated to TM-27 in the LGdM record (Figure 7 d-e, Figure 8 c-d), which in turn has been correlated to the X-6 marine tephra (Wulf et al., 2006; 2012). The X-6, first recognised in Ionian Sea marine cores, has been attributed to an unknown Campanian source (Keller et al., 1978). More recently, correlatives of the X-6 tephra have been identified in Ionian Sea core KC01B (Insinga et al., 2014) and terrestrially it is recognised in the San Gregorio Magno basin, Italy (Munno and Petrosino, 2007), Lake Ohrid, located on the Albania/Macedonia border (Sulpizio et al., 2010; Vogel et al., 2010) and in the Sulmona basin (Regattieri et al., 2015) (Figure 7d and e). An interpolated age of  $107 \pm 2$  ka has been assigned to the X-6 tephra in the Ionian Sea (Kraml, 1997), but more recently has been dated by  $^{40}\text{Ar}/^{39}\text{Ar}$  to  $108.9 \pm 1.8$  ka BP (Iorio et al., 2014); both age estimates are in good agreement with the TM-27 varve age of 108,430 years BP obtained from the LGdM chronology (Brauer et al., 2007). PRAD-2812 lies in a period of increased  $\delta^{18}\text{O}$  associated with MIS 5.4 stadial conditions (Figure 3), which is consistent with the occurrence of TM-27 in the Melisey 1 stadial at LGdM (Brauer et al., 2007) and the stratigraphic position of the X-6 in the Sulmona basin (Regattieri et al., 2015). Consequently, the PRAD 2812/TM-27 tephra provides a crucial isochron that not only has a diagnostic LAR glass chemistry, but is also stratigraphically well constrained. If this reasoning is correct, then identification of the X-6

tephra in the PRAD 1-2 record would extend the known northern dispersal range of this important marker.

**PRAD-3225** has a potential source from Vico as the majority of the data plots in or along the same trend as the Vico field (Figure 6b). It shows greatest affinity with TM-38 in the LGdM sequence, RF95-7 322cm from the Adriatic Sea and OT0701-7 from Lake Ohrid. TM-38 does not show the same trend in data as PRAD-3225 but does correlate with the main geochemical grouping (Figure 7f and supplementary data). TM-38 is described as being of Campanian origin by Wulf et al. (2012) but no proximal equivalent has so far been found, it is dated to c.  $125.6 \pm 6.3$  ka by the LGdM chronology. However, there are some discrepancies in the stratigraphic position of TM-38 and PRAD-3225. In LGdM TM-38 is deposited at the start of the Last Interglacial, although the layer is deposited just prior to when the percentages of Mediterranean and mesic woody taxa decline suddenly. This decline suggests the environment deteriorates rapidly just after the deposition of TM-38a, when woody taxa could not be supported, which has been interpreted as indicating an interval of hot summers and seasonal moisture deficiency (Brauer et al., 2007). However PRAD-3225 is deposited near the end of MIS 6, where there is a light oxygen isotope peak, just prior to a rapid excursion to heavier isotope values, which also indicated a rapid environmental deterioration (Figure 3). Therefore there are differences in the stratigraphic stage that TM-38 and PRAD-3225 occur in but closer examination of the records suggest similarities between the marine and terrestrial environmental responses at this time (Figure 3).

Tephra RF95-7 322 has been linked with the Carbognano Formation, the co-ignimbrite ash related to the pumice flows of the Ignimbrite D unit of Vico (Calanchi and Dinelli, 2008). Unfortunately significant discrepancies exist between the direct age determinations for this

eruptive unit, indeed Turbeville (1992) date this co-ignimbrite deposit to  $120 \pm 6$  ka, whilst Laurenzi and Villa (1987) derived an age of  $138 \pm 2$  ka. Consequently, it becomes difficult to confidently ascribe an age to PRAD-3225 based on its correlation to RF95-7 322 and associated links to the Vico Ignimbrite D. .

PRAD-3225 also shows geochemical affinities with tephra layer OT0701-7 from Lake Ohrid (Figure 7f). This layer was correlated to the X-5 by Sulpizio et al. (2010), based on one population of the OT0701-7 geochemical data. Nevertheless it is clear that the full OT0701-7 geochemical range shows closer similarities to the PRAD-3225 and RF95-7 322 cm data (Figure 7f) than to the X-5 tephra and its correlatives or to other CVZ tephra layers of a similar age (e.g. PRAD-2525 and PRAD-2605) (Figure 7b and c).

Due to the difference in ages for the Vico unit and whilst that inferred for TM-38 is uncertain due to stratigraphic inconsistencies no age estimate for PRAD-3225 has been incorporated into the age model presented below.

**PRAD-3336** could have a potential source from either the CVZ (Figure 6a) or Vico (Figure 6b), but when compared to tephra layers in LGdM that are older than TM-38, it has no clear correlative (Figure 10a). It resembles most closely the layer at 335 cm in the RF95-7 record (Figure 10b) although the latter has been tentatively correlated to the W-1 layer of Keller et al. (1978) (Calanchi and Dinelli, 2008). However, PRAD-3336 shows no similarities to the I-10 tephra which was also tentatively correlated to the W-1 by Insinga et al. (2014) (Figure 10bi). That aside, the correlation to the W-1 is supported by comparison with raw data from the W-1 layer in the METEOR core M25/4-12 from the Ionian Sea (Figure 10c). The W-1 is found in Ionian Sea cores (Keller et al., 1978) and also in the Eastern Mediterranean

(Vezzoli, 1991) and sits within sediments attributed to MIS-6, between sapropels 5 and 6, which is stratigraphically consistent with the position of PRAD-3336.

**PRAD-3383** yields geochemical data that lie within the CVZ field in Figure 6a but not within one of the source fields represented in Figure 6b, instead aligning more closely with the Vico field. The layer can be correlated to TM-39 (Figure 7f), which Wulf et al. (2012) describe as being of Campanian origin, although they do not assign it to a specific eruption. TM-39, which is dated by the LGdM chronology to c.  $130.5 \pm 6.5$  ka, has not previously been detected in a distal marine sequence.

**PRAD-3472** has a possible source from the CVZ (Figure 6a and b). It cannot be correlated to any of the remaining layers in LGdM (Wulf et al., 2012) nor with any of the tephra layers in core RF95-7 from the Adriatic Sea (Calanchi and Dinelli, 2008) or in core KC01B from the Ionian Sea (Insinga et al., 2014) (Figure 10a-b). PRAD-3472 is stratigraphically positioned at the end of S-E6 (Figure 3) (Piva et al., 2008a and b) and could therefore provide a useful marker for testing the degree to which S-E6 is contemporaneous with sapropel 6 in the wider Mediterranean, if it can be detected in other sequences.

**PRAD-3586** has a potential source from Vico (Figure 6b) and whilst it does not match any of the remaining layers in LGdM (Figure 10a) it does match the tephra layer detected between 419 – 410 cm depth in the RF95-7 sequence (Figure 10b) (Calanchi and Dinelli, 2008). Both layers also show affinity with the V-2 layer of Keller et al. (1978) (Figure 10c). The V-2 layer is found within sapropel 6 in the Ionian Sea cores, which is consistent with PRAD-3586 lying within S-E6, supporting the view that these sapropel layers are synchronous (Piva et al., 2008a, b).

Calanchi and Dinelli (2008) correlate the 419-410 cm layer with phonolitic pumiceous deposits of the Sutri Formation from Vico volcano which have been dated by  $^{40}\text{Ar}/^{39}\text{Ar}$  to  $151 \pm 3$  ka (Laurenzi and Villa, 1987). Palladino et al., (2014) also correlate the RF95-7 419-410 cm to the “Tufo Rosso a Scorie Nere Vicano” (WIC) eruption of Vico (another name for the Sutri Formation). Glass data from the WIC eruption (Palladino et al., 2014) and whole rock geochemical data from the Sutri Formation (Perini et al., 2004) show close similarities between this unit and the data obtained from PRAD-3586, RF95-6 419-410 cm, and the V-2 layer (Figure 10c). The estimated age of the WIC/Sutri Formation is c. 20 kyr younger than the age (170 ka) estimated for the V-2 layer (Narcisi and Vezzoli, 1999) and there are no documented eruptions of Vico with an age of 170 ka BP (Bear et al., 2009) with the Ronciglione formation ( $157 \pm 3$  ka) (Laurenzi and Villa, 1987) and the Casale de Monte lavas ( $250 \pm 50$  ka) (Sollevanti, 1983). Given these off-sets, an age estimate for the Sutri Formation was not incorporated into the age model for PRAD 1-2.

**PRAD-3666** also has a potential source from Vico volcano (Figure 6b) and can be correlated to the 450 cm tephra layer in the RF95-7 sequence (Calanchi and Dinelli, 2008) (Figure 10b). RF95-7 450 cm is not correlated to a known eruption but is thought to be related to Roman activity and possibly that of Vico (Calanchi and Dinelli, 2008). PRAD-3666 is associated with the onset of S-E 6 (Figure 3) (Piva et al., 2008a and b), and therefore could be an important marker layer if found in other archives.

## **6. Age Model and its Implications**

In order to constrain the ages of palaeoenvironmental events in PRAD 1-2 and to generate age estimates for the previously undetected tephra layers an age model for MIS5 and MIS 6



500 in PRAD 1-2 was generated in two stages. The first stage sought to determine the most  
 501 precise age estimates for previously-recognised tephra layers and the second applied the  
 502 results to the PRAD 1-2 record. Four of the tephra layers detected in PRAD 1-2 were also  
 503 represented in LGdM, and the established ages of these layers were employed in a *Sequence*  
 504 model using Oxcal v4.2 (Bronk Ramsey, 2009). As LGdM is an annually-laminated record,  
 505 the varve ages assigned to the layers can be used to estimate the duration of the intervals  
 506 between them, providing additional constraints for age model construction, the output from  
 507 which is presented in Table 1 and the code of the model is available in the supplementary  
 508 data. Once the age estimates were optimised using this approach, the results were used to  
 509 generate a *P\_Sequence* model (Bronk Ramsey, 2008) for the PRAD 1-2 record. The *P-*  
 510 *Sequence* algorithm incorporates relative depth information to allow an age-depth model for  
 511 the PRAD 1-2 sequence to be constructed (Blockley et al., 2008). An additional date  
 512 incorporated into this model is that for the Iceland Basin magnetic excursion (IBE) further  
 513 constraining the older part of the sequence (Table 2). The IBE has been dated via orbital  
 514 tuning to ca. 188 ka BP (Laj et al., 2006) but an independent K-Ar date of  $191 \pm 17$  ka has  
 515 also been obtained for this excursion, recorded in Japanese lava (Yamamoto et al., 2010): the  
 516 latter age estimate was incorporated into the age model to avoid ages derived using tuning  
 517 techniques. *Boundary* functions were placed where marked changes in lithology were  
 518 observed in the PRAD 1-2 sequence (Piva et al., 2008a). Where tephra layers could be  
 519 assigned to specific eruption events, the ages of corresponding events were assigned to the  
 520 position of peak tephra content in the case of cryptotephra layers, and with the base of visible  
 521 layers. The thickness of the visible tephra layers have been subtracted from the model to  
 522 make it event-free as tephra layers are deposited instantaneously. Where no dates were  
 523 available for an identified tephra layer, an age was interpolated using the final age model

(Table 2). The final output of the model is illustrated in Figure 11 with key steps summarised in Table 2 and the model code presented in the supplementary data.

The age model suggests an age for PRAD-3225 of 121 – 139 ka. This layer was correlated to RF94-7-322 cm and therefore to Ignimbrite D from Vico, which had 2 differing age estimates of  $120 \pm 6$  ka (Turbeville, 1992) and  $138 \pm 2$  ka (Laurenzi and Villa, 1987). The age generated for PRAD-3225 encompasses both of these ages, supporting the correlation but indicating that more proximal analysis and dating of this unit needs to be undertaken to resolve the age discrepancies. PRAD-3225 also shows geochemical similarities to TM-38 but their respective stratigraphic positions are not wholly consistent. The age generated for PRAD-3225 is also consistent with the varve age for TM-38 ( $125.6 \pm 6.3$  ka Wulf et al., 2012), supporting the geochemical correlation but the age range for PRAD-3225 needs to be refined before a firmer correlation can be made. PRAD-3336, which was correlated to the W-1 layer of Keller et al. (1978), is dated to 127 – 142 ka BP. This is in agreement with the estimated age of 140 ka BP of Narcisi and Vezzoli (1999), and therefore represents the first direct age estimate of a layer correlated to the W-1 tephra layer.

The final age model is free from regional biostratigraphic and climatic assumptions (such as those generated through the use of tuning or alignment techniques) and can therefore be used to compare the ages of global and regional environmental and climatic transitions, previously assumed by Piva et al. (2008a and b) to be synchronous across the Mediterranean. For example, the PRAD 1-2 record contains sapropel-equivalent (S-E) events which Piva et al. (2008a and b) assume to be synchronous with the Eastern Mediterranean sapropels. Three of these events occur in the period covered by the final PRAD 1-2 age model, S-E4, 5 and 6. In the Eastern Mediterranean the midpoints of Sapropel 4 (S4) and Sapropel 6 (S6) are dated via

orbital tuning in the Ionian Sea record KC01B to c. 101 ka BP and c. 172 ka BP respectively (Lourens, 2004); in addition, Bard et al., (2002) date Sapropel 6 to between 170 and 180 ka BP. The total age range of sapropel 5 (S5) is generally agreed to be between 124 and 119 ka BP (Bar-Matthews et al., 2000). The depth with the lowest  $\delta^{18}\text{O}$  values associated with each S-E event was used as the tie-point by Piva et al. (2008a), and for consistency the ages of these midpoints will be queried using the independent PRAD 1-2 age model. For the S-E4, S-E5 and S-E6 events these depths are 27.30 m, 30.60 m and 35.30 m respectively (Piva et al., 2008a). These are dated by the new age model to between 109.5 and 99.6 ka BP, 136.6 and 108.4 ka BP and 162.8 and 132.9 ka BP respectively (Table 2). The ages for S-E4 and S-E5 in PRAD 1-2 are consistent with the sapropel ages in the wider Mediterranean, supporting the proposals of Piva et al., (2008a).

However the age estimate for S-E6 is younger than the age of c. 172 ka BP derived for S6 by Lourens (2004) using orbital tuning, the age offset being similar to that between the age of the Sutri Formation (ca 151 ka) and the V-2 tephra layers (170 ka) which geochemically match the glass from PRAD-3586. The age model gives an age for PRAD-3586 (which occurs within S-E6) of 160.5 – 132.4 ka BP, which supports the correlation of this layer to the Sutri formation, dated by  $^{40}\text{Ar}/^{39}\text{Ar}$  to  $151 \pm 3$  ka BP (which was not included in the age-model). Hence both the dated proximal unit and the age for PRAD-3586 derived from the independent age model presented above are consistent in suggesting that S-E6 and sapropel 6 are more likely to date to c. 151 ka BP than to the previously-assumed age of 172 ka. This interpretation is advanced only tentatively, however, for the proposed correlation between the PRAD-3586, the V-2 ash layers and the WIC/Sutri formation needs to be tested more robustly. Moreover, it is possible that the PRAD-3586 and V-2 layers were derived from an older eruption of Vico, although no evidence for an older eruption has yet been documented.

Another possibility is that there is a hiatus within the PRAD 1-2 sequence, with the result that the age model under-estimates the age of the sediments at around 3586 cm depth, although no evidence for a significant hiatus was reported by Piva et al. (2008a or b). On the other hand, evidence from the Soreq cave speleothem record, which suggests a correlation between minimum speleothem  $\delta^{18}\text{O}$  peaks and sapropel events, could have a bearing on this matter (Bar-Matthews et al., 2000). While that record shows a pronounced low  $\delta^{18}\text{O}$  event dating to around 178 ka, and which is assumed to correlate with sapropel 6, it also shows another distinct  $\delta^{18}\text{O}$  minimum which dates to c. 152 ka. Furthermore a speleothem record from the Tan ache Urla cave, central Italy also shows evidence for enhanced rainfall at  $153.1 \pm 1.9$  ka (Regattieri et al., 2014). Both of these events are considered equivalent to the monsoon index maximum at c. 151 ka (Ayalon et al., 2002), which would also accord with our revised age estimate for S-E6. Taking the evidence as a whole, therefore, there may be a case for re-examination of the currently assumed age of S6. The dating of sapropel layers has hitherto mainly relied on orbital tuning, an approach that generates age estimates that are too coarse for establishing their precise timing (Emeis et al., 2003). This study is one of the first to directly date sediment thought to be equivalent to sapropel layers, and raises the possibility that the orbitally-tuned age for S6 of c. 172 ka is an overestimate.

The new age model presented here allows a comparison of the tuning points used by Piva et al. (2008a) to construct their age model (Table 3). Termination II in PRAD 1-2 is dated to 111.4 – 137.0 ka BP, which is in agreement with the age for Termination II from Lisiecki and Raymo (2005) and for the onset of the interglacial in LGdM of 127 ka BP (Brauer et al., 2007). Furthermore, local speleothem records suggest the transition from the penultimate glacial to the last interglacial to date to c.  $132.1 \pm 1.8$  ka (Regattieri et al., 2014) which also supports the age suggested by the PRAD 1-2 age model. The age generated for MIS 5.4

(105.4 – 111.1 ka BP) is in agreement with the age of Martinson et al., 1987 and with the age proposed for the Melisey 1 stadial in LGdM (109.5-107.6 ka) (Brauer et al., 2007). Likewise the age suggested for MIS 5-2 (85.1-88.2 ka) agrees (within errors) with the age of the Melisey 2 stadial in LGdM (87.98-90.65). It is, however, younger than the Martinson et al., (1987) age, although no age uncertainties are provided for the latter, so a precise comparison is not possible. These and other discordancies with orbitally-tuned age estimates can only be resolved by additional independent age control, with tephra isochrones potentially providing one of the most potent means of synchronising marine records within the Mediterranean.

Finally, the correlation of PRAD-3586 and the V-2 to the Sutri Formation, dated to  $151 \pm 3$  ka BP, also has implications for Mediterranean tephrostratigraphy as the Kos Plateau Tuff (W-3) has been  $^{40}\text{Ar}/^{39}\text{Ar}$  dated to  $161 \pm 2$  ka BP (Bachmann et al., 2010), which is older than the age for the V-2 proposed here. It should be noted, however, that the W-3 and V-2 ash layers have not been found in the same sequences, and hence the superposition of these layers is assumed rather than tested. As the V-2 has not been directly dated until now, and there is no known superposition of the W-3 and V-2 layers, the age of the V-2 proposed here cannot be discounted on present evidence

## **7. Conclusions**

Eleven tephra layers have been identified within the part of the PRAD 1-2 sequence assigned on biostratigraphic and sapropel layer stratigraphy to MIS 5 and 6 (Table 4). Of these eleven, five can be correlated confidently on geochemical characteristics to tephra layers identified in Lago Grande di Monticchio, three of which (PRAD-2375/TM-22, PRAD-3336/TM-38 and PRAD-3383/TM-39) represent the first distal occurrences of these layers. In all three cases the new data extends their known distributions approximately 210 km further north (Table 4).

Of the remaining six tephra layers, three can be correlated to layers identified in core RF95-7 (Calanchi and Dinelli, 2008), with PRAD-3336 and PRAD-3586 also being correlated to the Mediterranean marker layers, W-1 and V-2 of Keller et al., (1978). The final three layers, detected for the first time, cannot presently be correlated with known events. Age estimates generated for these tephra layers (Table 4) can be imported should equivalent layers be detected in other sequences in future studies. The age model produced for these PRAD 1-2 tephra layers provides direct age estimates for sapropel-equivalent events in the Adriatic Sea that for the first time are independent of orbital tuning models. The results indicate that orbitally-tuned ages for some events during MIS-5 to 6 are insufficiently constrained.

Of the tephra layers reported here, the X-6/PRAD-2812/TM-27 best meets the criteria specified in section 1 and hence is considered the most useful isochron: it is the only layer that is robustly chemically characterised, chemically distinctive, widespread, robustly dated, and provides secure constraints for an event of interest – in this case MIS 5.4 in marine sequences and the Melisey 1 stage in Mediterranean terrestrial sequences (Brauer et al., 2007). The X-5 tephra which has been considered to be a regional marker layer (Giaccio et al., 2012) has been shown not to be geochemically unique in its major element composition: at least 4 compositionally-similar tephra layers occur during the same period. Thus unless all layers are present in a single record it would not be possible to use them for the correlation and synchronisation of archives without good stratigraphic control, independent ages and additional trace element analyses. PRAD-3586/V-2 is geochemically distinctive, constrains sapropel 6 and is widespread within the Mediterranean Sea, but the age of this layer is uncertain. PRAD-2375/TM-22 is also geochemically distinctive and constrains an event of interest (MIS5.2) though it has not yet proved to be widespread. Of the other layers identified in PRAD 1-2, all are robustly chemically characterised and chemically distinctive, and can be

assigned firm age estimates, but while PRAD-3666 also constrains an event of interest (S-E6), only PRAD-3336/W-1 has yet been widely traced. Further work is therefore needed to explore their wider potential.

Finally within the 16 m of sediment analysed in this study, eight of the eleven layers are visible horizons, whereas in the 21 m of overlying sediment analysed by Bourne et al., (2010) none of the twenty layers identified were visible horizons. This could reflect the fact that many of layers identified here originate from Vico, which is more proximal to PRAD 1-2 than the CVZ, while the absence of visible layers in the upper segments of the core relate to the dominance of activity further south (in the CVZ) during the 0-90 ka period. Other factors such as a change in prevailing wind direction or the possibility that these earlier eruptions from the CVZ and Vico may have been larger-scale eruptions than the more recent well-studied eruptions discussed in Bourne et al., (2010), could also explain the difference observed in number of visible horizons.

## **Acknowledgements**

Core PRAD 1-2 was recovered from the western flank of the Central Adriatic basin within the PROMESS 1 European Project (PROfiles across Mediterranean Sedimentary Systems) funded by EU contract no. EVR1-CT-2002-40024. AJB's research on the PRAD 1-2 core was funded in part by the CNR-ISMAR, Bologna, and in part by a Thomas Holloway studentship award from Royal Holloway University of London. PGA's contribution was funded by the NERC RESET Consortium Project (NE/E015905/1) and all of the research has benefitted from association with this project. We would like to thank Dr Alison MacLeod for her assistance with geochemical analysis of the samples, Dr Chris Hayward for his assistance with the use of the electron microprobe at the Tephrochronology Analytical Unit, University

of Edinburgh and Norman Charnley for his assistance with the use of the electron microprobe at the Department of Earth Sciences, University of Oxford. Thanks also to Helen Adams for her assistance with laboratory work and Enrico Dinelli for providing normalised glass-specific data for the RF95-7 sequence. We are grateful to Roberto Sulpizio and 2 anonymous reviewers for their detailed comments on earlier drafts that have greatly improved this manuscript. This paper forms RHOXTOR contribution number 041.

## References

- Ayalon, A., Bar-Matthews, M., Kaufman, A., 2002. Climatic conditions during marine oxygen isotope stage 6 in the eastern Mediterranean region from the isotopic composition of speleothems of Soreq Cave, Israel. *Geology* 30, 303-306.
- Bachmann, O., Schoene, B., Schnyder, C., Spikings, R., 2010. The  $^{40}\text{Ar}/^{39}\text{Ar}$  and U/Pb dating of young rhyolites in the Kos-Nisyros volcanic complex, Eastern Aegean Arc, Greece: Age discordance due to excess  $^{40}\text{Ar}$  in biotite. *Geochemistry, Geophysics, Geosystems* 11, Q0AA08.
- Bard, E., Delaygue, G., Rostek, F., Antonioli, F., Silenzi, S., Schrag, D., 2002. Hydrological conditions in the western Mediterranean basin during the deposition of Sapropel 6 (ca 175 kyr). *Earth and Planetary Science Letters* 202, 481-494.
- Bar-Matthews, M., Ayalon, A., Kaufman, A., 2000. Timing and hydrological conditions of Sapropel events in the Eastern Mediterranean, as evident from speleothems, Soreq cave, Israel. *Chemical Geology* 169, 145-156.
- Bear, A.N., Cas, R.A.F., Giordana, G., 2009. Variations in eruptive style and depositional processes associated with explosive, phonolitic composition, caldera-forming eruptions: The



698 151 ka Sutri eruption, Vico Caldera, central Italy. *Journal of Volcanology and Geothermal*  
699 *Research* 184, 225-255

700 Blockley, S.P.E., Pyne-O'Donnell, S.D.F., Lowe, J.J., Matthews, I.P., Stone, A., Pollard,  
701 A.M., Turney, C.S.M., Molyneux, E.G., 2005. A new and less destructive laboratory  
702 procedure for the physical separation of distal glass tephra shards from sediments. *Quaternary*  
703 *Science Reviews* 24, 1952-1960.

704 Blockley, S.P.E., Ramsey, C.B., Lane, C.S., Lotter, A.F., 2008. Improved age modelling  
705 approaches as exemplified by the revised chronology for the Central European varved lake  
706 Soppensee. *Quaternary Science Reviews* 27, 61-71.

707 Bourne, A.J., Lowe, J.J., Trincardi, F., Asioli, A., Blockley, S.P.E., Wulf, S., Matthews, I.P.,  
708 Piva, A., Vigliotti, L., 2010. Distal tephra record for the last ca 105,000 years from core  
709 PRAD 1-2 in the central Adriatic Sea implications for marine tephrostratigraphy. *Quaternary*  
710 *Science Reviews* 29, 3079-3094.

711 Brauer, A., Mingram, J., Frank, U., Gunter, C., Schettler, G., Wulf, S., Zolitschka, B.,  
712 Negendank, J.F.W., 2000. Abrupt environmental oscillations during the Early Weichselian  
713 recorded at Lago Grande di Monticchio, southern Italy. *Quaternary International* 73-4, 79-90.

714 Brauer, A., Allen, J.R.M., Mingram, J., Dulski, P., Wulf, S., Huntley, B., 2007. Evidence for  
715 last interglacial chronology and environmental change from Southern Europe. *Proceedings of*  
716 *the National Academy of Sciences of the United States of America* 104, 450-455.

717 Bronk Ramsey, C., 2008. Deposition models for chronological records. *Quaternary Science*  
718 *Reviews* 27, 42-60.

719 Bronk Ramsey, C., 2009. Bayesian Analysis of Radiocarbon Dates. *Radiocarbon* 51, 337-  
720 360.

721 Calanchi, N., Cattaneo, A., Dinelli, E., Gasparotto, G., Lucchini, F., 1998. Tephra layers in  
722 Late Quaternary sediments of the central Adriatic Sea. *Marine Geology* 149, 191-209.

723 Calanchi, N., Dinelli, E., 2008. Tephrostratigraphy of the last 170 ka in sedimentary  
724 successions from the Adriatic Sea. *Journal of Volcanology and Geothermal Research* 177,  
725 81-95.

726 Caron, B., Sulpizio, R., Zanchetta, G., Siani, G., Santacroce, R., 2010. The Late Holocene to  
727 Pleistocene tephrostratigraphic record of Lake Ohrid (Albania). *Comptes Rendus Geoscience*  
728 342, 453-466.

729 Davies, S.M., Elmquist, M., Bergman, J., Wohlfarth, B., Hammarlund, D., 2007.  
730 Cryptotephra sedimentation processes within two lacustrine sequences from west central  
731 Sweden. *Holocene* 17, 319-330.

732 Davies, S.M., Abbott, P.M., Pearce, N.J.G., Wastegard, S., Blockley, S.P.E., 2012.  
733 Integrating the INTIMATE records using tephrochronology: rising to the challenge.  
734 *Quaternary Science Reviews* 36, 11-27.

735 Emeis, K.C., Schulz, H., Struck, U., Rossignol-Strick, M., Erlenkeuser, H., Howell, M.W.,  
736 Kroon, D., Mackensen, A., Ishizuka, S., Oba, T., Sakamoto, T., Koizumi, I., 2003. Eastern  
737 Mediterranean surface water temperatures and  $\delta^{18}\text{O}$  composition during deposition of  
738 sapropels in the late Quaternary. *Paleoceanography* 18.

739 Giaccio, B., Nomade, S., Wulf, S., Isaia, R., Sottili, G., Cavuoto, G., Galli, P., Messina, P.,  
740 Sposato, A., Sulpizio, R., Zanchetta, G., 2012. The late MIS 5 Mediterranean tephra markers:  
741 a reappraisal from peninsular Italy terrestrial records. *Quaternary Science Reviews* 56, 31-45.

742 Griggs, A.J., Davies, S.M., Abbott, P.M., Rasmussen, T.L., Palmer, A.P., 2014. Optimising  
743 the use of marine tephrochronology in the North Atlantic: a detailed investigation of the  
744 Faroe Marine Ash Zones II, III and IV. *Quaternary Science Reviews*, 106, 122–139.

745 Hayward, C., 2012. High spatial resolution electron probe microanalysis of tephra and melt  
746 inclusions without beam-induced chemical modification. *Holocene* 22, 119-125.

747 Hunt, J.B., Hill, P.G., 1993. Tephra geochemistry: a discussion of some persistent analytical  
 748 problems. *The Holocene* 3, 271-278.

749 Insinga, D.D., Tamburrino, S., Lirer, F., Vezzoli, L., Barra, M., De Lange, G.J., Tiepolo, M.,  
 750 Vallefucio, M., Mazzola, S., Sprovieri, M., 2014. Tephrochronology of the astronomically-  
 751 tuned KC01B deep-sea core, Ionian Sea: insights into the explosive activity of the Central  
 752 Mediterranean area during the last 200 ka. *Quaternary Science Reviews* 85, 63-84.

753 Iorio, M., Sagnotti, L., Angelino, A., Budillon, F., D'Argenio, B., Dinares-Turell, J., Macri,  
 754 P., Marsella, E., 2014. High-resolution petrophysical and palaeomagnetic study of late-  
 755 Holocene shelf sediments, Salerno Gulf, Tyrrhenian Sea. *Holocene* 14, 426-435.

756 Jochum, K.P., Nohl, U., Herwig, K., Lammel, E., Stoll, B., Hofmann, A.W., 2005. GeoReM:  
 757 A new geochemical database for reference materials and isotopic standards. *Geostand  
 758 Geoanal Res* 29, 333-338.

759 Jochum, K.P., Willbold, M., 2006. Reference materials in geoanalytical research - Review for  
 760 2004 and 2005. *Geostand Geoanal Res* 30, 143-156.

761 Keller, J., Ryan, W.B.F., Ninkovich, D., Altherr, R., 1978. Explosive Volcanic Activity in  
 762 Mediterranean over Past 200,000 Yr as Recorded in Deep-Sea Sediments. *Geological Society  
 763 of America Bulletin* 89, 591-604.

764 Kraml, M., 1997. Laser-40Ar/39Ar-Datierungen an distalen marinen Tephren des jung-  
 765 quartären mediterranen Vulkanismus (Ionisches Meer, METEOR-Fahrt 25/4). *Albert-  
 766 Ludwigs-Universit.at Freiburg*, p. 216.

767 Laj, C., Kissel, C., Roberts, A.P., 2006. Geomagnetic field behavior during the Iceland Basin  
 768 and Laschamp geomagnetic excursions: A simple transitional field geometry? *Geochemistry  
 769 Geophysics Geosystems* 7.

770 Lane, C.S., Blockley, S.P.E., Mangerud, J., Smith, V.C., Lohne, O.S., Tomlinson, E.L.,  
 771 Matthews, I.P., Lotter, A.F., 2012. Was the 12.1 ka Icelandic Vedde Ash one of a kind?  
 772 Quaternary Science Reviews 33, 87-99.  
 773 Laurenzi, M., Villa, I., 1987.  $^{40}\text{Ar}/^{39}\text{Ar}$  chronostratigraphy of Vico ignimbrites. Per. Mineral  
 774 56, 285-293.  
 775 Le Bas, M.J., Le Maitre, R.W., Streckeisen, A., Zanettin, B., 1986. A chemical classification  
 776 of volcanic rocks based on the Total Alkali-Silica diagram. Journal of Petrology 27, 745–750.  
 777 Lisiecki, L.E., Raymo, M.E., 2005. A Pliocene-Pleistocene stack of 57 globally distributed  
 778 benthic delta O-18 records. Paleoceanography 20.  
 779 Lourens, L.J., 2004. Revised tuning of Ocean Drilling Program Site 964 and KC01B  
 780 (Mediterranean) and implications for the delta O-18, tephra, calcareous nannofossil, and  
 781 geomagnetic reversal chronologies of the past 1.1 Myr. Paleoceanography 19.  
 782 Lowe, D.J., 2011. Tephrochronology and its application: A review. Quaternary  
 783 Geochronology 6, 107-153.  
 784 Martinson, D.G., Pisias, N.G., Hays, J.D., Imbrie, J., Moore, T.C., Shackleton, N.J., 1987.  
 785 Age dating and the orbital theory of the Ice Ages: Development of a high-resolution 0–  
 786 300,000 year chronostratigraphy. Quaternary Research 27, 1-29.  
 787 Munno, R., Petrosino, P., 2007. The late Quaternary tephrostratigraphical record of the San  
 788 Gregorio Magno basin (southern Italy). Journal of Quaternary Science 22, 247-266.  
 789 Narcisi, B., Vezzoli, L., 1999. Quaternary stratigraphy of distal tephra layers in the  
 790 Mediterranean - an overview. Global and Planetary Change 21, 31-50.  
 791 Negri A, Capotondi L, Keller J. 1999. Calcareous nannofossils, planktonic foraminifera and  
 792 oxygen isotopes in the late Quaternary sapropels of the Ionian Sea. Marine Geology 157: 89–  
 793 103.

794 Palladino, D.M., Agosta, E., Freda, C., S., S., Trigila, R., 1994. Geo-petrographic and  
 795 volcanological study of Southern Vulsini: the Valentano-Marta-La Rocca sector. Mem.  
 796 Descr. Carta Geol. Ital. XLIX, 255–276.

797 Palladino D.M., Gaeta M., Giaccio B., Sottili G. 2014. On the anatomy of magma chamber  
 798 and caldera collapse: The example of trachy-phonolitic explosive eruptions of the Roman  
 799 Province (central Italy). *Journal of Volcanology and Geothermal Research* 281, 12-26.

800 Pappalardo, L., Civetta, L., D' Antonio, M., Deino, A., Di Vito, M., Orsi, G., Carandente, A.,  
 801 de Vita, S., Isaia, R., Piochi, M., 1999. Chemical and Sr-isotopical evolution of the Phlegrean  
 802 magmatic system before the Campanian Ignimbrite and the Neapolitan Yellow Tuff  
 803 eruptions. *Journal of Volcanology and Geothermal Research* 91, 141-166.

804 Paterne, M., Guichard, F., Labeyrie, J., 1988. Explosive activity of the south Italian  
 805 volcanoes during the past 80,000 years as determined by marine tephrochronology *Journal of*  
 806 *Volcanology and Geothermal Research* 34, 153-172.

807 Paterne, M., Labeyrie, J., Guichard, F., Mazaud, A., Maitre, F., 1990. Fluctuations of the  
 808 Campanian explosive volcanic activity (South Italy) during the past 190,000 years, as  
 809 determined by marine tephrochronology *Earth and Planetary Science Letters* 98, 166-174.

810 Paterne, M., Guichard, F., Duplessy, J.C., Siani, G., Sulpizio, R., Labeyrie, J., 2008. A  
 811 90,000-200,000 yrs marine tephra record of Italian volcanic activity in the Central  
 812 Mediterranean Sea. *Journal of Volcanology and Geothermal Research* 177, 187-196.

813 Peccerillo, A., 2005. *Plio-Quaternary Volcanism in Italy*. Springer.

814 Perini, G., Francalanci, L., Davidson, J.P., Conticelli, S., 2004. Evolution and Genesis of  
 815 Magmas from Vico Volcano, Central Italy: Multiple Differentiation Pathways and Variable  
 816 Parental Magmas. *Journal of Petrology* 45, 139 - 182.

817 Piva, A., Ascoli, A., Schneider, R.R., Trincardi, F., Andersen, N., Colmenero-Hidalgo, E.,  
 818 Dennielou, B., Flores, J.A., Vigliotti, L., 2008a. Climatic cycles as expressed in sediments of

819 the PROMESS1 borehole PRAD1-2, central Adriatic, for the last 370 ka: 1. Integrated  
820 stratigraphy. *Geochemistry Geophysics Geosystems* 9.

821 Piva, A., Asioli, A., Andersen, N., Grimalt, J.O., Schneider, R.R., Trincardi, F., 2008b.  
822 Climatic cycles as expressed in sediments of the PROMESS1 borehole PRAD1-2, central  
823 Adriatic, for the last 370 ka: 2. Paleoenvironmental evolution. *Geochemistry Geophysics*  
824 *Geosystems* 9.

825 Pyne-O'Donnell, S., 2011. The taphonomy of Last Glacial-Interglacial Transition (LGIT)  
826 distal volcanic ash in small Scottish lakes. *Boreas* 40, 131-145.

827 Regattieri E., Zanchetta G., Drysdale R.N., Isola I., Hellstrom J.C., Roncioni A. 2014. A  
828 continuous stable isotopic record from the Penultimate glacial maximum to the Last  
829 Interglacial (160 to 121 ka) from Tana Che Urla Cave (Apuan Alps, central Italy). *Quaternary*  
830 *Research*, 82, 450-461.

831 Regattieri E., Giaccio B., Zanchetta G., Drysdale R.N., Galli P., Nomade S., Peronace E.,  
832 Wulf S. 2015. Enhanced rainfall seasonality over Apennine during the late MIS 5 precession  
833 minimum as revealed by a stable isotope record from Sulmona basin, central Italy. *Journal of*  
834 *Quaternary Science*, 30(1), 19-31.

835 Ridente, D., Trincardi, F., Piva, A., Asioli, A., Cattaneo, A., 2008. Sedimentary response to  
836 climate and sea level changes during the past similar to 400 ka from borehole PRAD1-2  
837 (Adriatic margin). *Geochemistry Geophysics Geosystems* 9.

838 Rosi, M., Sbrana, A., 1987. Phlegrean Fields. Consiglio Nazionale delle Ricerche, Roma.

839 Rotolo, S.G., Scaillet, S., La Felice, S., Vita-Scaillet, G., 2013. A revision of the structure and  
840 stratigraphy of pre-Green Tuff ignimbrites at Pantelleria (Strait of Sicily). *Journal of*  
841 *Volcanology and Geothermal Research* 250, 61-74.

842 Sánchez Goñi, M., Cacho, I., Turon, J., Guiot, J., Sierro, F., Peyrouquet, J., Grimalt, J.,  
843 Shackleton, N., 2002. Synchronicity between marine and terrestrial responses to millennial

844 scale climatic variability during the last glacial period in the Mediterranean region. *Climate*  
845 *Dynamics* 19, 95-105.

846 Santacroce, R., Cioni, R., Marianelli, P., Sbrana, A., Sulpizio, R., Zanchetta, G., Donahue,  
847 D.J., Joron, J.L., 2008. Age and whole rock–glass compositions of proximal pyroclastics  
848 from the major explosive eruptions of Somma-Vesuvius: A review as a tool for distal  
849 tephrostratigraphy. *Journal of Volcanology and Geothermal Research* 177, 1-18.

850 Sollevanti, F., 1983. Geologic, Volcanologic and tectonic setting of the Vico-Cimino Area,  
851 Italy. *Journal of Volcanology and Geothermal Research* 17, 203–217.

852 Smith, V.C., Isaia, R., Pearce, N.J.G., 2011. Tephrostratigraphy and glass compositions of  
853 post-15 ka Campi Flegrei eruptions: implications for eruption history and chronostratigraphic  
854 markers. *Quaternary Science Reviews* 30, 3638-3660.

855 Sulpizio, R., Zanchetta, G., D'Orazio, M., Vogel, H., Wagner, B., 2010. Tephrostratigraphy  
856 and tephrochronology of lakes Ohrid and Prespa, Balkans. *Biogeosciences* 7, 3273-3288.

857 Tamburrino S., Insinga D., Sprovievri M., Petrosino P., Tiepolo M. 2012. Major and trace  
858 element characterization of tephra layers offshore Pantelleria Island: insights into the last 200  
859 ka of volcanic activity and contribution to the Mediterranean tephrochronology. *Journal of*  
860 *Quaternary Science* 27(2) 129-140.

861 Tomlinson, E.L., Thordarson, T., Muller, W., Thirlwall, M., Menzies, M.A., 2010.  
862 Microanalysis of tephra by LA-ICP-MS - Strategies, advantages and limitations assessed  
863 using the Thorsmork ignimbrite (Southern Iceland). *Chemical Geology* 279, 73-89.

864 Tomlinson, E.L., Arienzo, I., Civetta, L., Wulf, S., Smith, V.C., Hardiman, M., Lane, C.S.,  
865 Carandente, A., Orsi, G., Rosi, M., Muller, W., Menzies, M.A., 2012. Geochemistry of the  
866 Phlegraean Fields (Italy) proximal sources for major Mediterranean tephras: Implications for  
867 the dispersal of Plinian and co-ignimbritic components of explosive eruptions. *Geochimica et*  
868 *Cosmochimica Acta* 93, 102-128.

869 Tomlinson, E.L., Albert, P.G., Wulf, S., Brown, R.J., Smith, V.C., Keller, J., Orsi, G.,  
 870 Bourne, A.J., Menzies, M.A., 2014. Age and geochemistry of tephra layers from Ischia, Italy:  
 871 constraints from proximal-distal correlations with Lago Grande di Monticchio. *Journal of*  
 872 *Volcanology and Geothermal Research*, 287, 22-39.  
 873 Trigila, R., 1995. The volcano of the Alban Hills. Tipografia della Scuola Grafica Salesiana,  
 874 Roma.  
 875 Turbeville, B.N., 1992.  $^{40}\text{Ar}/^{39}\text{Ar}$  Ages and stratigraphy of the Latera caldera, Italy. *Bulletin*  
 876 *of Volcanology* 55, 110-118.  
 877 Vezzoli, L., 1988. Island of Ischia, Quad. Ric. Sci. C.N.R., Roma, p. 126 pp.  
 878 Vezzoli, L., 1991. Tephra layers in Bannock Basin (Eastern Mediterranean). *Marine Geology*  
 879 100, 21-34.  
 880 Vogel, H., Zanchetta, G., Sulpizio, R., Wagner, B., Nowaczyk, N., 2010. A  
 881 tephrostratigraphic record for the last glacial-interglacial cycle from Lake Ohrid, Albania and  
 882 Macedonia. *Journal of Quaternary Science* 25, 320-338.  
 883 Wagner, B., Sulpizio, R., Zanchetta, G., Wulf, S., Wessels, M., Daut, G., Nowaczyk, N.,  
 884 2008. The last 40 ka tephrostratigraphic record of Lake Ohrid, Albania and Macedonia: a  
 885 very distal archive for ash dispersal from Italian volcanoes. *Journal of Volcanology and*  
 886 *Geothermal Research* 177, 71-80.  
 887 Webster, J.D., Raia, E., Tappen, C., De Vivo, B., 2003. Pre-eruptive geochemistry of the  
 888 ignimbrite-forming magmas of the Campanian Volcanic Zone, Southern Italy, determined  
 889 from silicate melt inclusions. *Mineralogy and Petrology* 79, 99 - 125.  
 890 Wulf, S., Kraml, M., Brauer, A., Keller, J., Negendank, J.F.W., 2004. Tephrochronology of  
 891 the 100 ka lacustrine sediment record of Lago Grande di Monticchio (southern Italy).  
 892 *Quaternary International* 122, 7-30.



893 Wulf, S., Brauer, A., Mingram, J., Zolitschka, B., Negendank, J.F.W., 2006. Distal tephras in  
 894 the sediments of Monticchio maar lakes. , In: Principe, C. (Ed.), *La geologia del Monte*  
 895 *Vulture*, Regione Basilicata. Consiglio Nazionale delle Ricerche, pp. 105–122.  
 896 Wulf, S., Keller, J., Paterne, M., Mingram, J., Lauterbach, S., Opitz, S., Sottili, G., Giaccio,  
 897 B., Albert, P.G., Satow, C., Tomlinson, E.L., Viccaro, M., Brauer, A., 2012. The 100-133 ka  
 898 record of Italian explosive volcanism and revised tephrochronology of Lago Grande di  
 899 Monticchio. *Quaternary Science Reviews* 58, 104-123.  
 900 Yamamoto, Y., Shibuya, H., Tanaka, H., Hoshizumi, H., 2010. Geomagnetic paleointensity  
 901 deduced for the last 300ka from Unzen Volcano, Japan, and the dipolar nature of the Iceland  
 902 Basin excursion. *Earth and Planetary Science Letters* 293, 236-249.  
 903

## Figure Captions

Figure 1: Synopsis of the stratigraphic positions of tephra layers of MIS 5 and 6 age reported from key tephrostratigraphical archives in the Central Mediterranean and of correlations between sites (dashed lines).

Figure 2: Location of PRAD 1-2 and the main Italian volcanic centres that were active during the Quaternary. The locations of the terrestrial and marine tephra sequences discussed in the text are also shown. LGdM = Lago Grande di Monticchio. Marine core locations are from Keller et al. (1978), Paterne et al. (1988, 2008), Calanchi et al. (1998, 2008). Terrestrial site locations are from Wulf et al. (2004, 2012) (LGdM), Giaccio et al., (2012) (Popoli and Le Saline), Munno and Petrosini. (2007) (San Gregorio Magno Basin), Wagner et al. (2008) (Lake Ohrid).

Figure 3: Multi-proxy information for core PRAD 1-2. A) Stratigraphic scheme, B) Lithology, C) Planktic (black curve) and benthic (blue curve) foram-based oxygen isotope record, D) Percentage of warm planktic foraminiferal species (red curve) E) ARM (blue curve) and SIRM (black curve) magnetic measures, F) Geomagnetic Inclination showing the position of the Iceland Basin excursion and G) Tephra layers identified for the section of PRAD 1-2 investigated in this study. Shading extends the MIS stratigraphic scheme across the diagram as a visual aid. Data provided by A. Asioli, L.Vigliotti and A. Piva and reported in Piva et al. (2008).

Figure 4: Photomicrographs showing the shard morphological characteristics of tephra layers, PRAD-2375 (A), PRAD-2525 (B), PRAD-2605 (C), PRAD-2812 (D), PRAD-3065 (E),

PRAD-3225 (F), PRAD-3336 (G), PRAD-3383 (H), PRAD-3472 (I), PRAD-3586 (J) and PRAD-3666 (K).

Figure 5: Total alkali vs. silica plot (Le Bas et al., 1986) for PRAD 1-2 tephra layers

Figure 6: A) Comparison of PRAD 1-2 layers with distinctive groupings of ash layers determined by alkali data. Volcanic system 1=Aeolian, 2=Campanian Volcanic Zone, 3=Ischia, 4=Pantelleria, 5=Etna, 6=Procida and 7=Alban Hills (reproduced from Paterne et al., 1988 and Wulf et al., 2004). B) CaO vs. MgO/TiO<sub>2</sub> used to discriminate the sources of PRAD 1-2 tephra layers. Fields 1-6 are defined by on-land volcanic products older than 60 ka based on data from (1) Campi Flegrei pre-Campanian Ignimbrite deposits, (2) Ischia pre-Monte Epomeo Green Tuff (Rosi and Sbrana (1987); Pappalardo et al. (1999); Tomlinson et al., (2014); Webster et al. (2003); Vezzoli (1988)); (3) the average composition of tephra layer X5 (Vezzoli (1991); Calanchi and Dinelli (2008)); (4) Vico (Perini et al., 2004; Palladino et al., 2014); (5) Vulsini (Tuberville (1992); Palladino et al. (1994)); and (6) Alban Hills (Trigila (1995); Peccerillo (2005) for the Roman area. Adapted from Calanchi and Dinelli (2008).

Figure 7: Major element biplots showing comparisons of PRAD 1-2 tephra layers. A) PRAD-2375 to LGdM (Wulf et al., 2012) and Pantelleria layers from Site 963A (Tamburrino et al., 2014). B) and C) PRAD-2525 and PRAD-2605 to LGdM (Wulf et al., 2012), Popoli and Le Saline (Giaccio et al., 2012; Regattieri et al., 2015) and Lake Ohrid layers (Sulpizio et al., 2010). D) and E) PRAD-2812 to LGdM (Wulf et al., 2012), Le Saline (Giaccio et al., 2012; POP4 (Regattieri et al., 2015), I-9 (Insinga et al., 2014) and Lake Ohrid layers (Sulpizio et

al., 2010). F) PRAD-3225 and PRAD-3383 to LGdM (Wulf et al., 2012), RF95-7 (Calanchi and Dinelli, 2008) and Lake Ohrid layers (Sulpizio et al., 2010).

Figure 8: Trace-element biplots showing comparison of PRAD 1-2 tephra layers with LGdM (Wulf et al., 2012) and Popoli layers (Giaccio et al., 2012). A) and B) PRAD-2525 and PRAD-2605, C) and D) PRAD-2812.

Figure 9: Harker diagrams of tephra layers in LGdM between TM-22 and TM-24 that are thicker than 0.5 cm, revealing the similarity of their major element compositions.

Figure 10: Comparison of PRAD-3336, PRAD-3472, PRAD-3586 and PRAD-3666 layers with A) Remaining layers in the LGdM sequence (Wulf et al., 2012). B) Layers from core RF95-7 from the Adriatic Sea (Calanchi and Dinelli, 2008). Normalised glass-specific data for the RF95-7 data was kindly provided by Enrico Dinelli. C) Comparison of PRAD 1-2 and RF95-7 layers with data from the W-1, V-2 (Keller et al., 1978), WIC (Palladino et al., 2014) and Sutri Formation (Perini et al, 2004).

Figure 11: 95.4% confidence Highest Probability Density output for the Bayesian age/depth model generated for the PRAD 1-2 sequence (based on a Poisson model). The model was constructed using the best constrained age estimates for the tephra layers identified in the sequence (Table 2). Boundaries were inserted at the top and base of the sequence.

Supplementary Figure 1: Harker Diagrams showing correlations of PRAD-3225 and PRAD-3383 to LGdM (Wulf et al., 2012), RF95-7 (Calanchi and Dinelli, 2008) and Lake Ohrid layers (Sulpizio et al., 2010).

978

979   Supplementary Information: A) Code from Oxcal *Sequence* model used to provide more  
980   precise age estimates for previously-recognised tephra layers. The intervals are based on the  
981   varve ages for the LGdM tephra layers and therefore the varve spacing between the layers  
982   (Wulf et al., 2012). The interval function is used to allow for uncertainty in the varve  
983   counting between the tephra layers (Brauer et al., 2000). B) Code from Oxcal *P\_Sequence*  
984   Model. The model used a variable k factor, the nominal k value  $k_0$  was 1 and this was  
985   allowed to vary by two orders of magnitude in either direction (Bronk Ramsey, 2008; 2009).

986

987

Table1

Table 1: Ages for the LGdM tephra layers correlated to PRAD 1-2 tephra layers (with  $2\sigma$  uncertainties) and varve spacings between the layers in LGdM used in the *Sequence* model (Unmodelled (BP) column) <sup>a</sup> =  $^{40}\text{Ar}/^{39}\text{Ar}$  dates with a  $1\sigma$  error and <sup>b</sup> = Monticchio varve ages with errors expressed as 5% of the date itself, as recommended by Brauer et al., (2000) (see text for details of individual dates). The refined age ranges for the tephra layers are shown in **bold** in the Modelled (BP) column. The A column shows the agreement index for each date

Name	Input Age Range		Modelled (BP)		Aoverall 87.4
			from	to	A
TM-22 (PRAD-2375) <sup>a</sup>	86696	83305	<b>86418</b>	<b>83142</b>	99.9
Interval N(10510,2380)	5750	15270	5141	11424	87.1
TM-23-11 (PRAD-2525) <sup>a</sup>	96990	87810	<b>96047</b>	<b>90069</b>	115
Interval N(17910,2710)	12490	23330	12276	19593	97.8
TM-27 (PRAD-2812) <sup>a</sup>	112492	105309	<b>112025</b>	<b>105957</b>	107.4
Interval N(33900,5085)	23730	44070	19577	35646	69.3
TM-39 (PRAD-3383) <sup>b</sup>	142473	118527	<b>144540</b>	<b>128597</b>	82.2

Table 2: OxCal model output for the PRAD 1-2 sequence. The Modelled (BP) column is the output for each date. The layers labelled in italics with a PRAD tephra code are layers that were not correlated to a known tephra layer and therefore could not be dated; therefore their age has been interpolated from the model. The A column shows the agreement index for each date.

Name	Unmodelled (BP)		%	Modelled (BP)		%	Aoverall 105.4 A	Depth (m)
	from	to		from	to			
Boundary <i>S3onset</i>				84679	80466	95.3		23.35
PRAD-2375/TM-22	86415	83146	95.4	86390	83217	95.4	101.2	23.75
<i>MIS5.2</i>				88234	85165	95.4		24.09
PRAD-2525/TM-23-11	96043	90074	95.4	95198	90915	95.4	114.2	25.25
<b><i>PRAD2605</i></b>				100686	94270	95.4		26.05
Boundary <i>S4onset</i>				109543	99640	95.3		27.30
<i>MIS5.4</i>				111135	105429	95.4		28.00
PRAD-2817/TM-27	112019	105964	95.4	111778	106053	95.4	102.3	28.12
Boundary <i>S5onset</i>				136593	108443	95.3		30.00
<b><i>PRAD3065</i></b>				136638	108912	95.4		30.60
<i>Termination II</i>				136936	111365	95.4		30.65
<b><i>PRAD-3225</i></b>				139162	121283	95.4		30.95
<i>MIS6.2</i>				139674	122893	95.4		32.25
<b><i>PRAD3336</i></b>				142369	127513	95.4		32.50
<i>MIS6.4</i>				143369	128539	95.4		33.36
PRAD-3383/TM-39	144543	128635	95.4	144859	129202	95.3	100.1	33.58
<b><i>PRAD3472</i></b>				151045	131171	95.4		33.83
<b><i>PRAD3586</i></b>				160474	132360	95.4		34.72
Boundary <i>S6onset</i>				162766	132891	95.4		35.30
PRAD-3666				181077	156346	95.4		35.86
Boundary IBE	213961	180041	95.4	210145	178301	95.5	95.0	37.28

Table 3: Comparison of the tuning points used at specific depths by Piva et al., (2008) in the construction of their age model and the modelled  $2\sigma$  age range for the same depths generated using the tephra age model.

<b>Depth (m)</b>	<b>Age (ka BP)</b>	<b>Source</b>	<b>Modelled Age (<math>2\sigma</math>)</b>
24.09	91	MIS 5.2 Martinson et al., (1987)	88234 - 85165
28.00	111	MIS 5.4 Martinson et al., (1987)	111135 - 105429
30.95	130	Termination II from Lisieki and Raymo (2005)	136936 - 111365
32.50	135	MIS 6.2 Martinson et al., (1987)	139674- 122893
33.58	152.5	MIS 6.4 Martinson et al., (1987)	143369 - 128539



Table4

Table 4: Summary of the tephra layers identified in PRAD 1-2, their correlation to Monticchio tephra layers and known volcanic events.  $n$  = number of geochemical determinations obtained. Classifications (based on Le Bas *et al.*, 1986): Tr = trachyte, P = phonolite, TP = tephriphonolite. Modelled  $2\sigma$  age range from Table 2.

PRAD 1-2 tephra	$n$	Classification	Monticchio tephra layer	RF95-7 tephra layer	Origin	Volcanic event	Published Date (ka BP)	Dating method	Modelled $2\sigma$ age (cal yr BP)
PRAD-2375	8	Unknown	TM-22	N/A	Pantelleria	Ignimbrite z unit	$79.3 \pm 4.2$	$^{40}\text{Ar}/^{39}\text{Ar}$	86,390 – 83,217
PRAD-2525	92	P/Tr	TM-23-11	N/A	CVZ	POP-1	$92.4 \pm 4.6$	$^{40}\text{Ar}/^{39}\text{Ar}$	95,198 – 90,915
PRAD-2605	28	P	Unknown	N/A	CVZ	N/A	N/A	N/A	100,686 – 94,270
PRAD-2812	27	P/Tr	TM-27	N/A	CVZ	X-6	$108.9 \pm 1.8$	$^{40}\text{Ar}/^{39}\text{Ar}$	111,778 – 106,053
PRAD-3065	N/A	N/A	Unknown	N/A	Unknown	Unknown	N/A	N?A	136,638 – 108,912
PRAD-3225	13	P	TM-38	322 cm	Vico	Ignimbrite D unit	$125.6 \pm 6.3$	Varves	139,162 – 121,283
PRAD-3336	10	P	Unknown	335 cm	Roman	W-1	140 ka	N/A	142,369 – 127,513
PRAD-3383	11	P/Tr	TM-39	N/A	CVZ	Unknown	$130.5 \pm 6.5$	Varves	144,859 – 129,202
PRAD-3472	11	Tr	N/A	N/A	Unknown	Unknown	N/A	N/A	151,045 – 131,171
PRAD-3586	10	P	N/A	410/419 cm	Vico	V-2 / Sutri Formation	$151 \pm 3.0$	$^{40}\text{Ar}/^{39}\text{Ar}$	160,474 – 132,360
PRAD-3666	10	P	N/A	450 cm	Latium	Unknown	N/A	N/A	181,077 – 156,346

Figure1

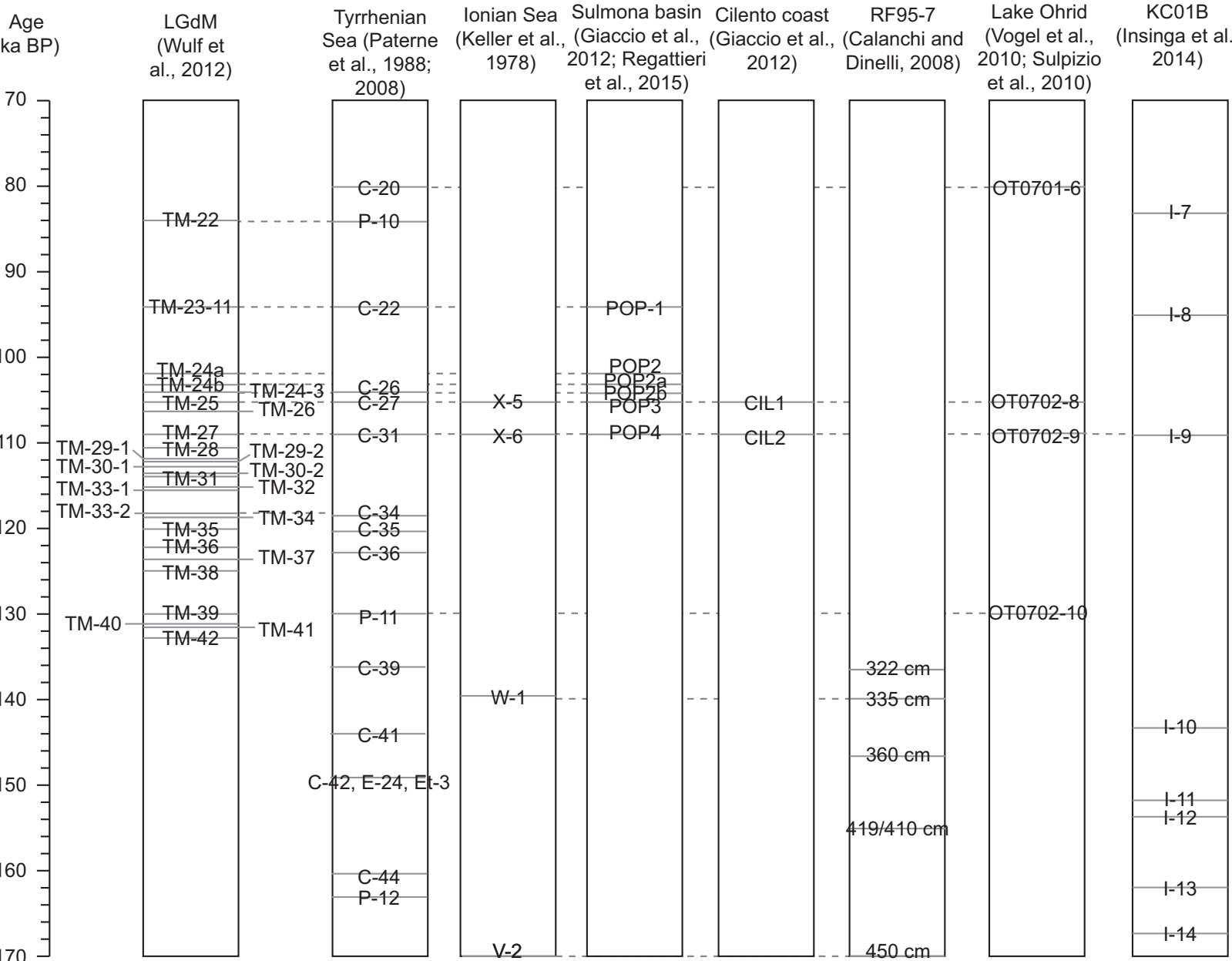


Figure2

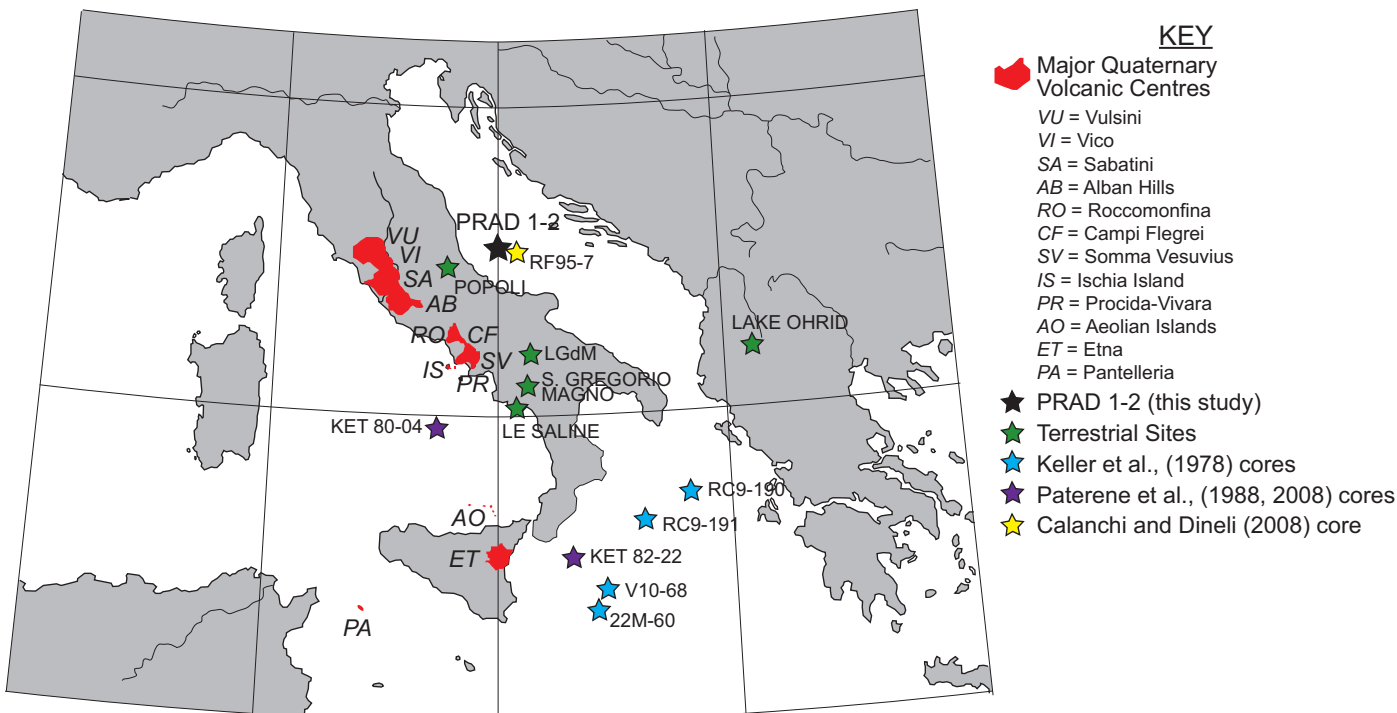


Figure3

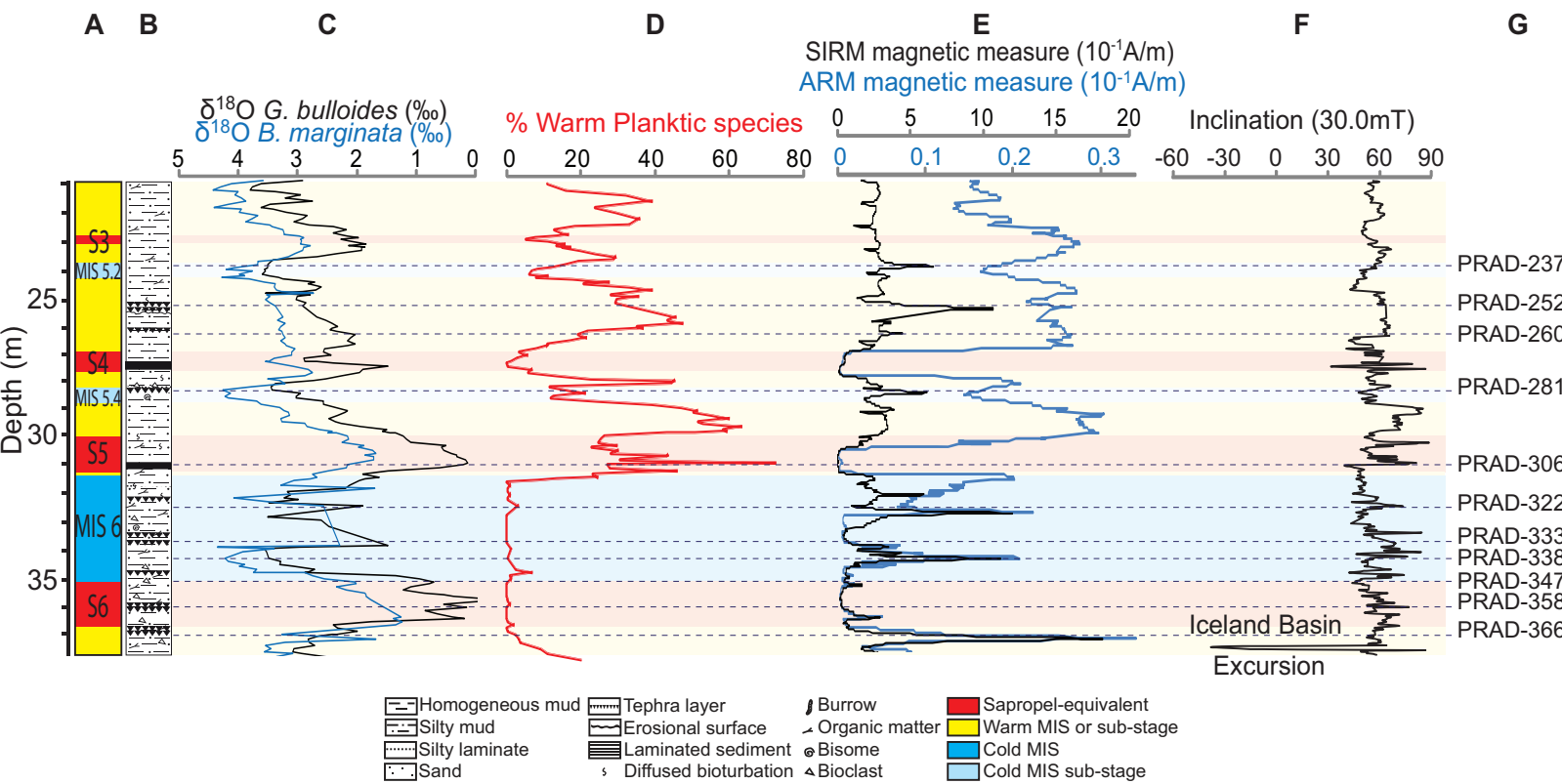


Figure4

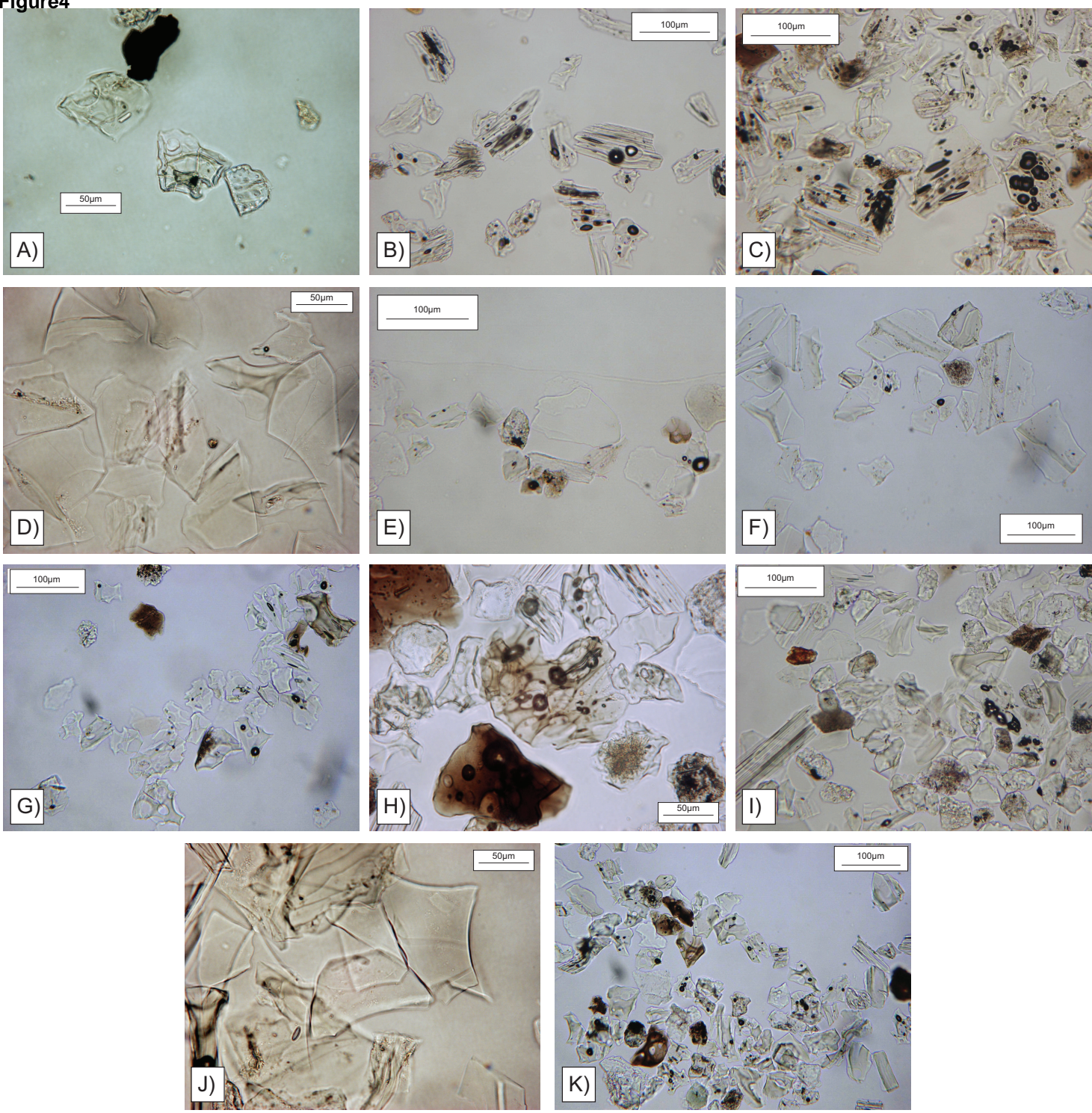




Figure5

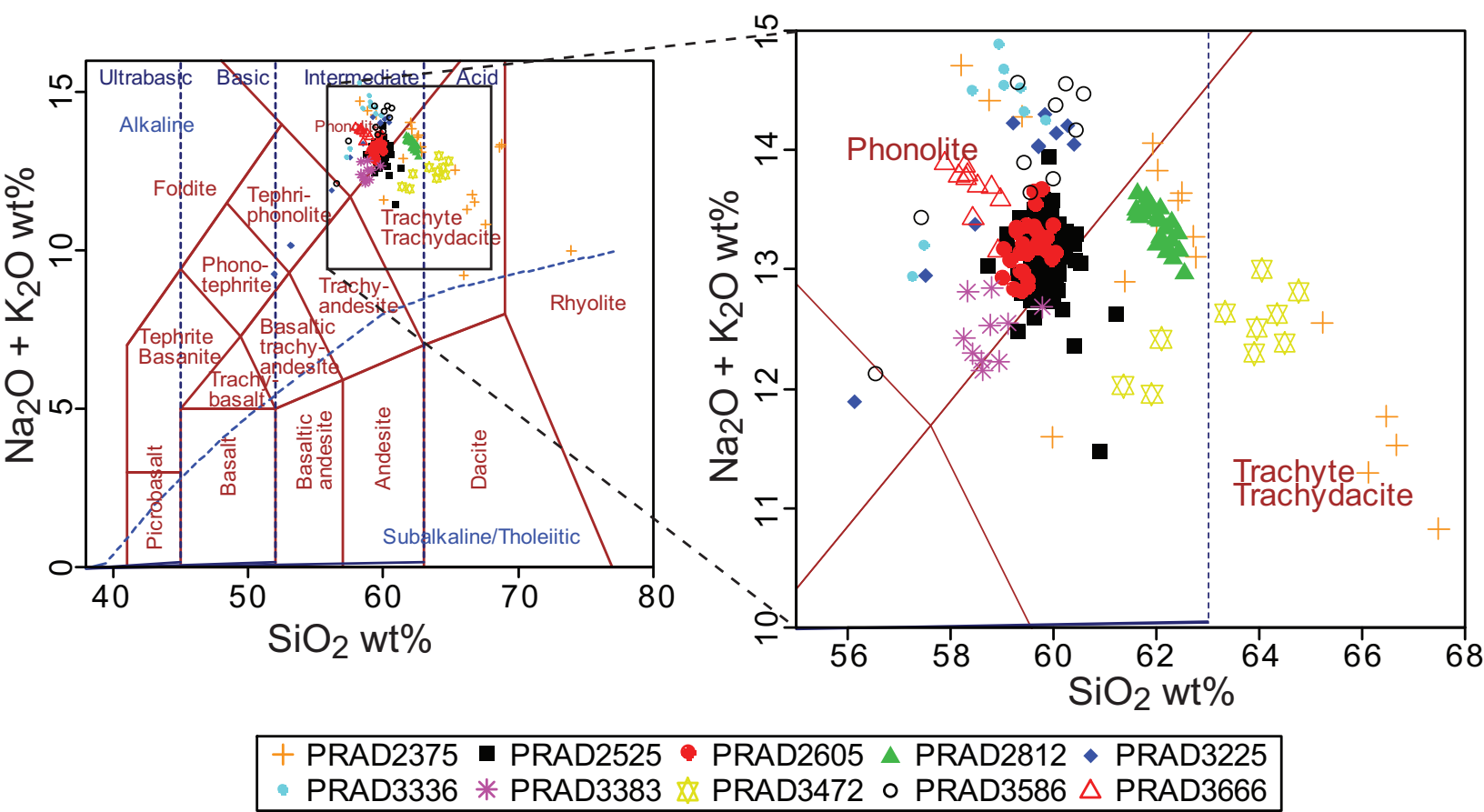
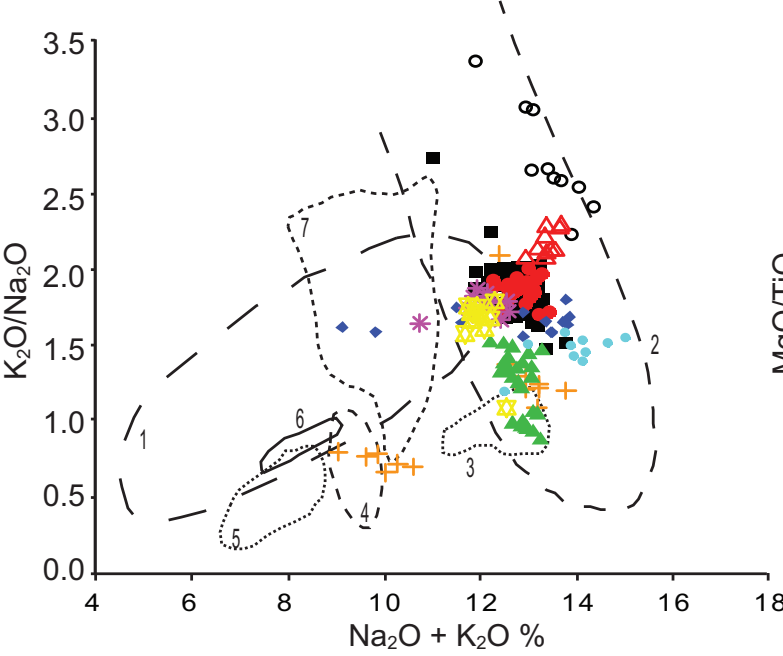


Figure6

**A**



**B**

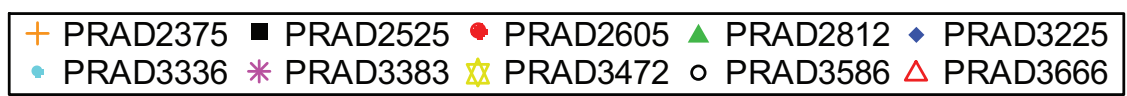
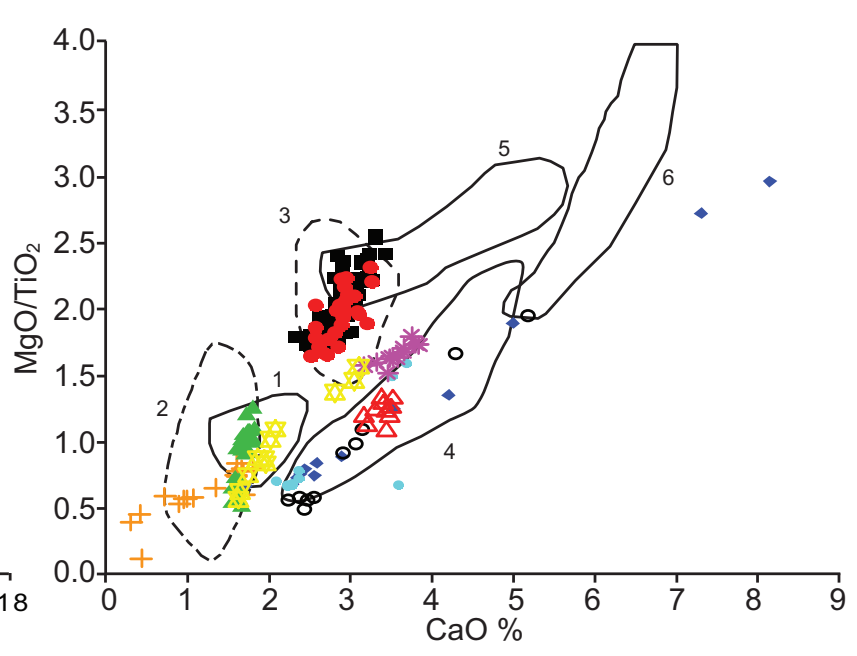


Figure7

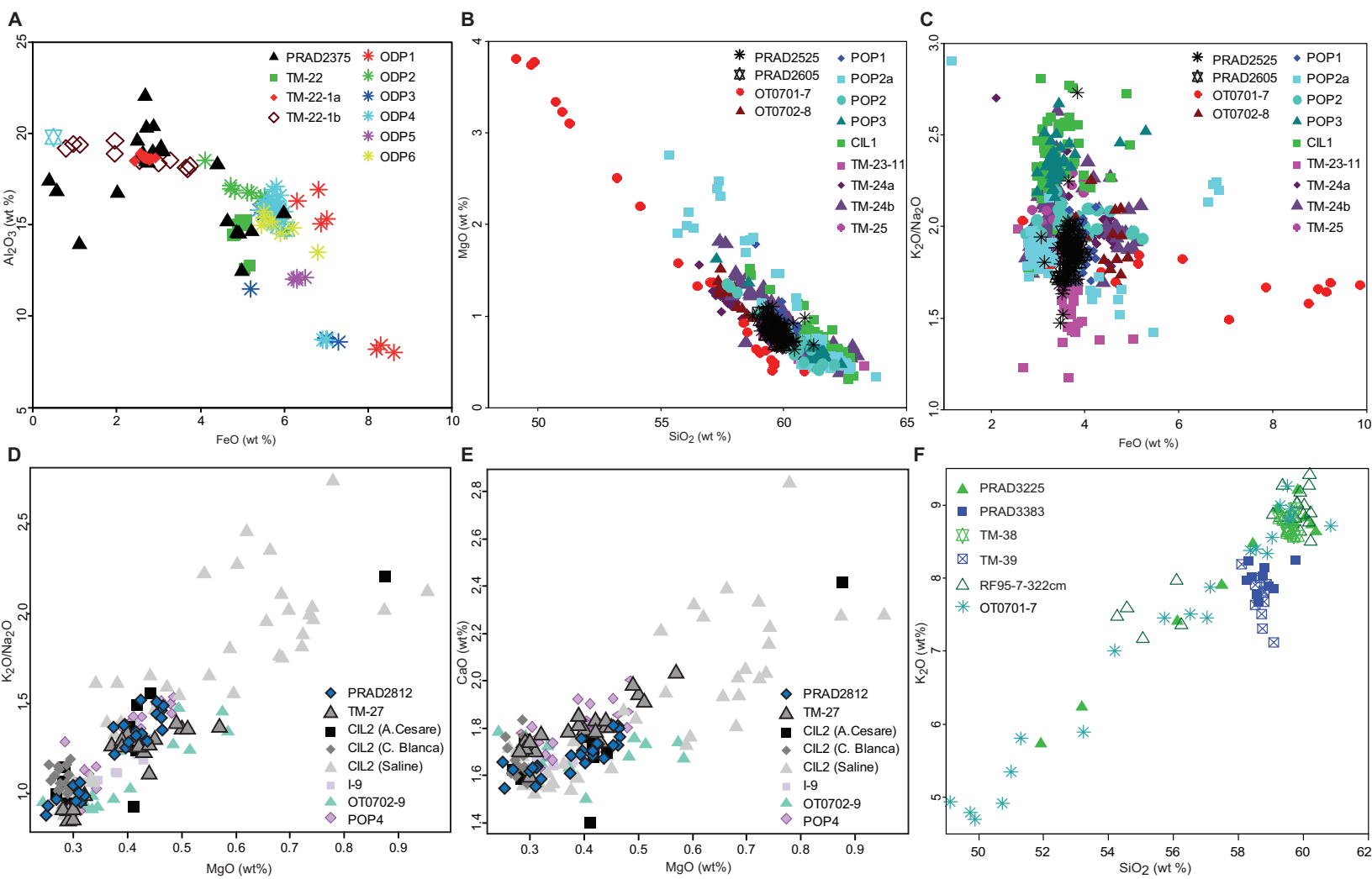




Figure8

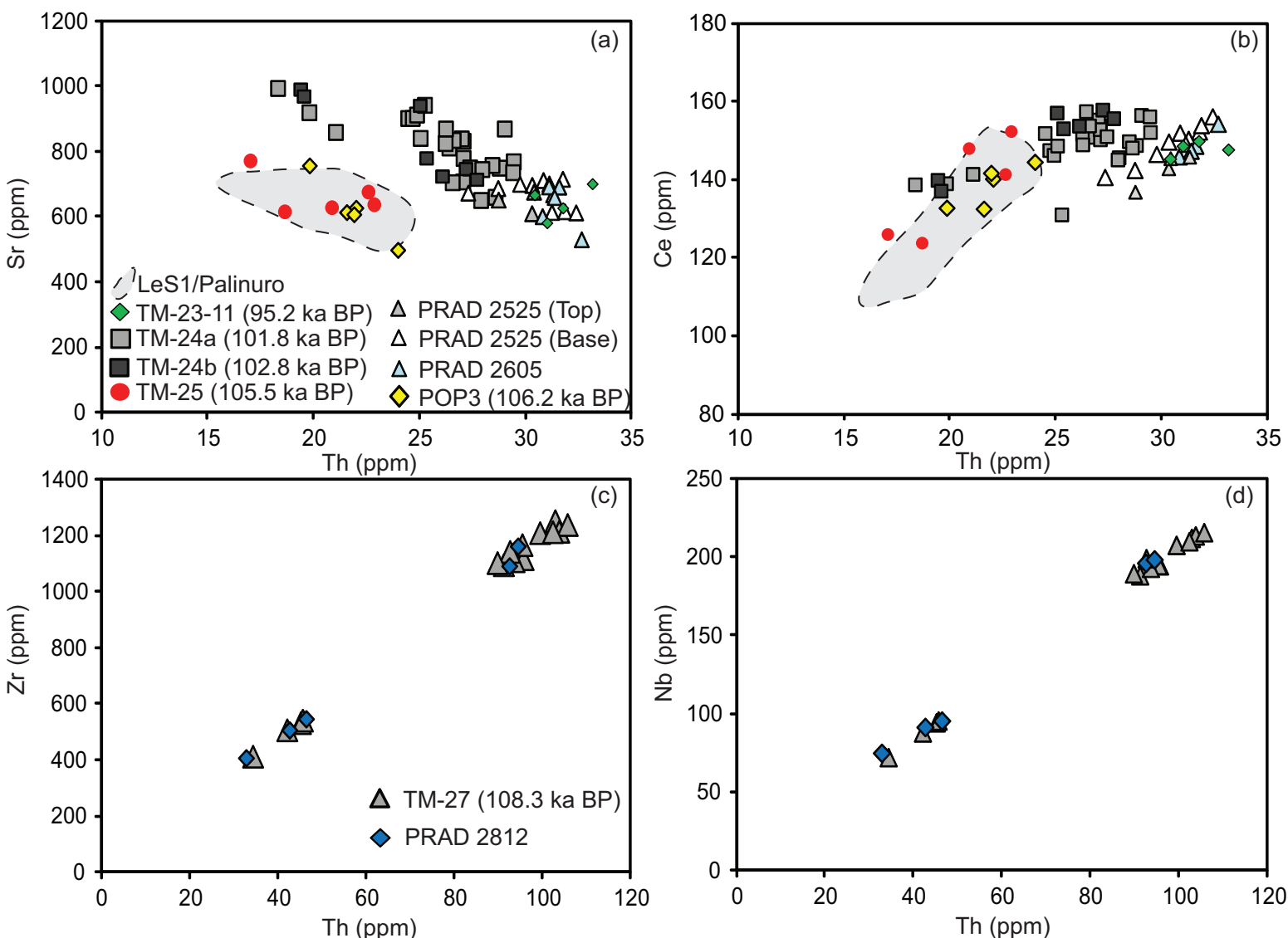


Figure9

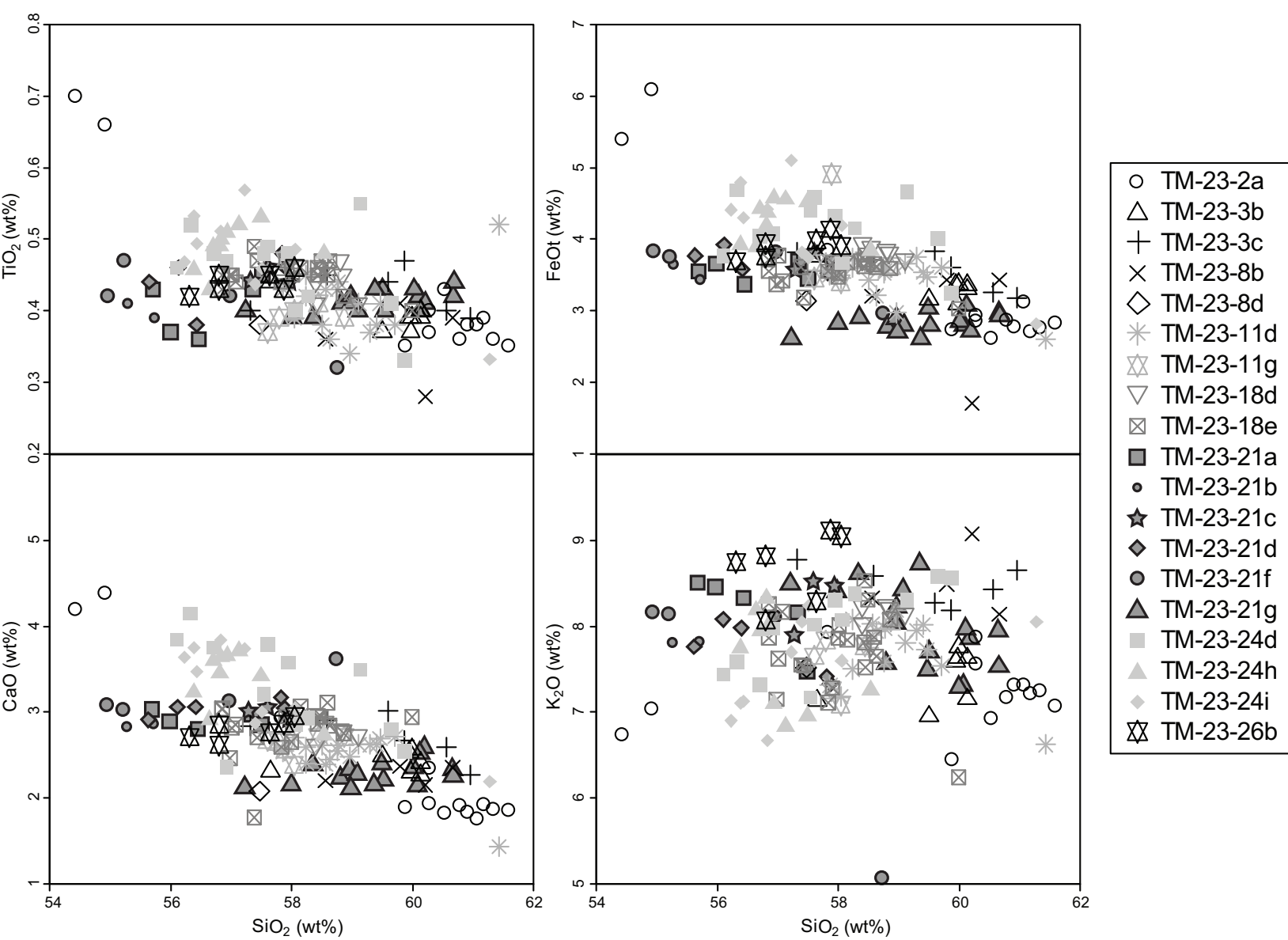
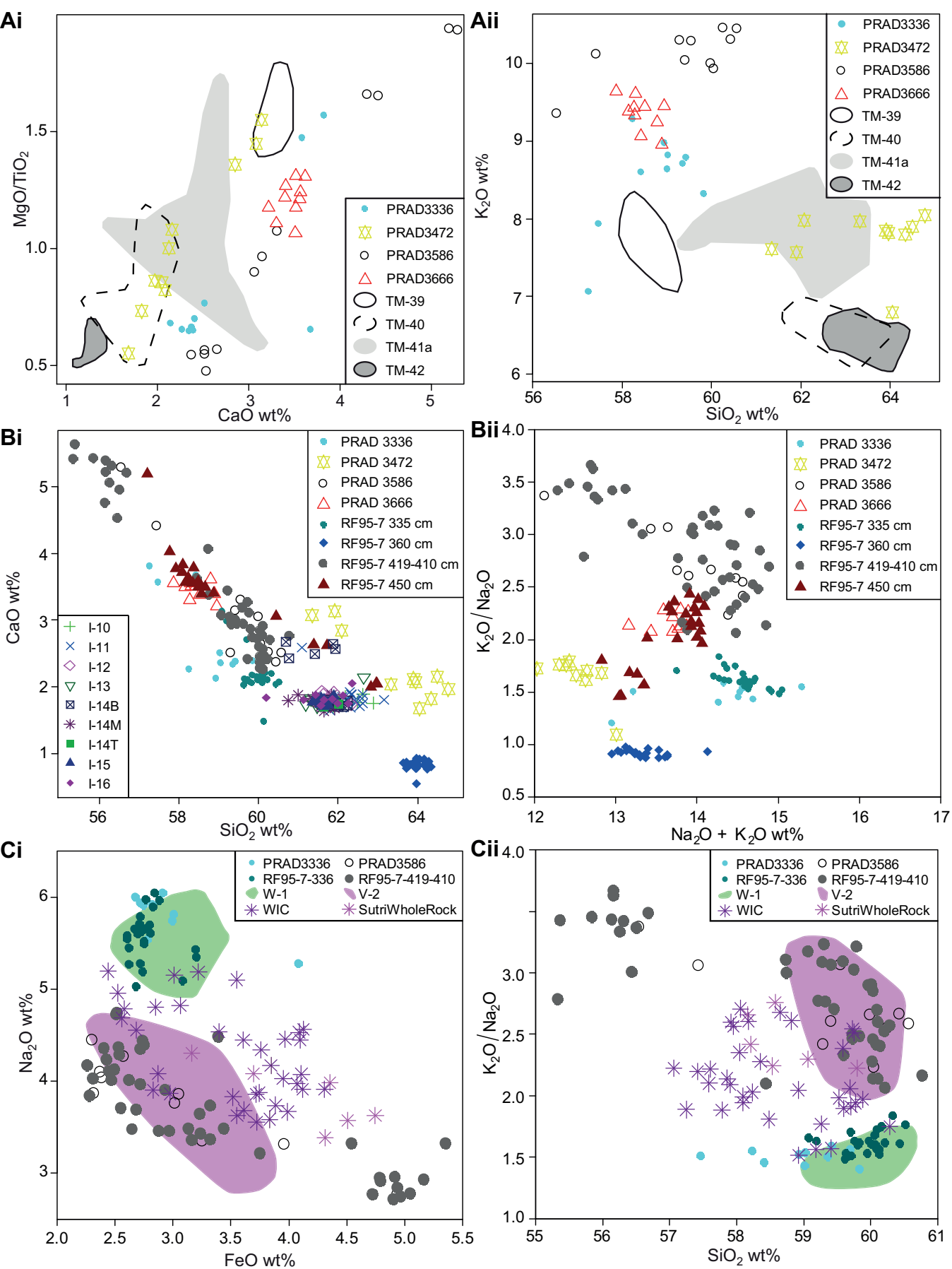
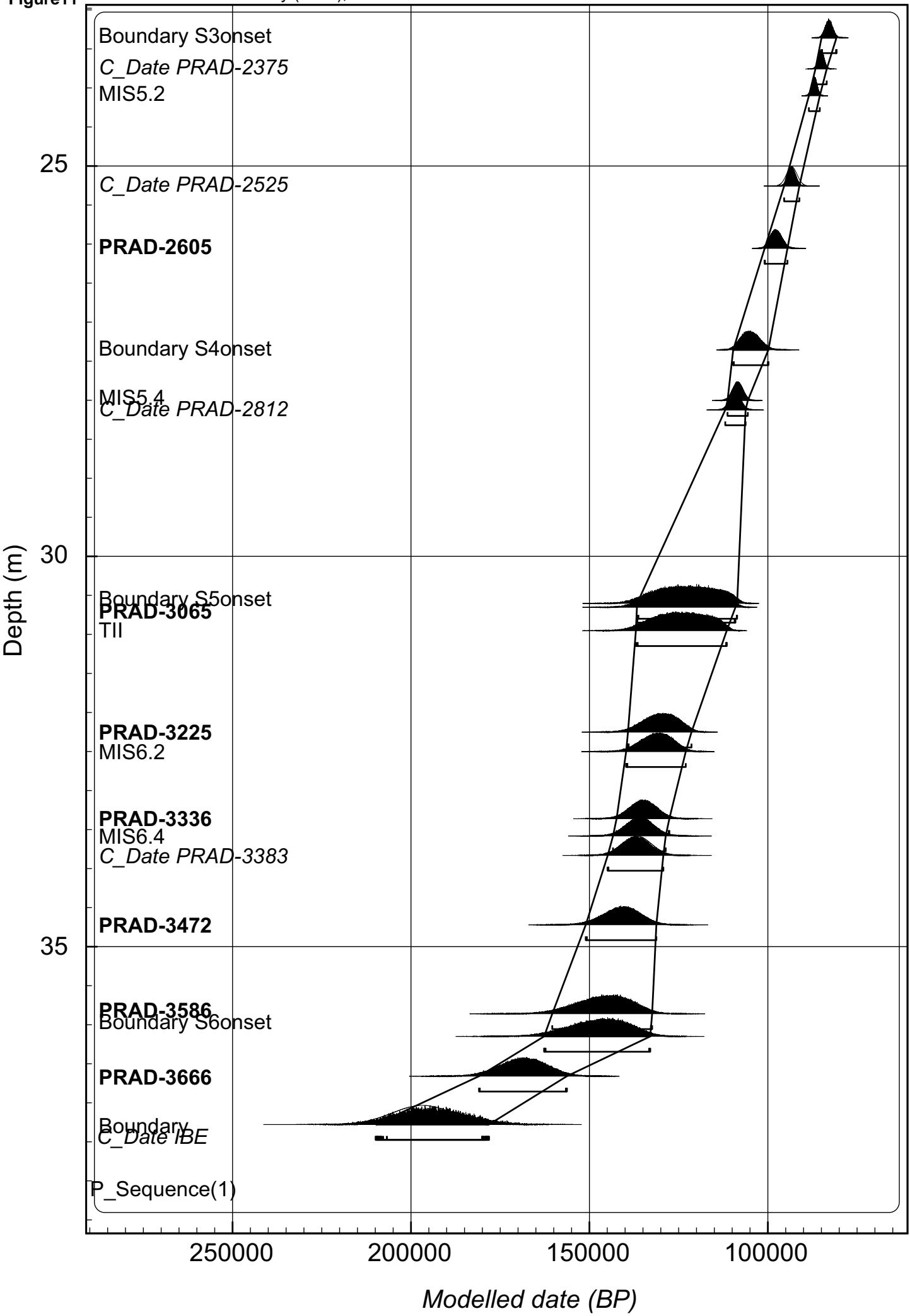


Figure10





**Supplementary Figure1**  
[Click here to download Supplementary Data: Supplementary Figure1.eps](#)

**Supplementary Information**

[Click here to download Supplementary Data: Supplementary Information.xlsx.docx](#)

**Supplementary Data**  
[Click here to download Supplementary Data: Supplementary Data.xlsx](#)